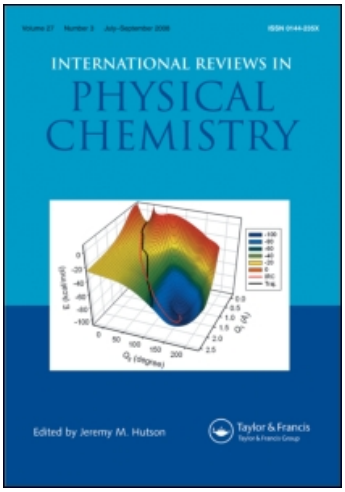

International Reviews in Physical Chemistry
Publication details, including instructions for authors and subscription information:
http://www.informaworld.com/smpp/title~content=t713724383

Analysis of highly excited vibrational eigenstates

Michael J. Davis[a]
[a] Chemistry Division, Argonne National Laboratory, Argonne, IL, USA

To cite this Article Davis, Michael J.(1995) 'Analysis of highly excited vibrational eigenstates', International Reviews in Physical Chemistry, 14: 1, 15 — 66
To link to this Article: DOI: 10.1080/01442359509353303
URL: http://dx.doi.org/10.1080/01442359509353303

INTERNATIONAL REVIEWS IN PHYSICAL CHEMISTRY, 1995, VOL. 14, NO. 1, 15–66

Analysis of highly excited vibrational eigenstates

by MICHAEL J. DAVIS

Chemistry Division, Argonne National Laboratory, Argonne, IL 60439, USA

Methods for the analysis of highly excited vibrational eigenstates are presented. These include semiclassical and hierarchical analyses, along with a discussion of the nature of eigenstates along a correlation diagram. The purpose of the analyses is to extract information from what often appear to be complicated, 'unassignable' eigenstates. In particular, I address how to rationalize the nature of eigenstates via the semiclassical analysis and how to extract information concerning assignability and energy flow from the hierarchical analysis. The study of the eigenstates along a correlation diagram, together with the semiclassical analysis, is undertaken to address the issue of the classical–quantum correspondence when the classical mechanics is chaotic.

1. Introduction

It is common in review papers to start by setting a general context for the research discussion in the article. I would like to start here a bit differently, discussing a specific set of results and leave the more general discussion for the next section. I wish to do this by presenting a figure that may strike many readers as overly complicated, and those who are uncomfortable with this are urged to start with §2 and come back here later.

Figure 1 shows a series of quantum eigenstates for system (2) defined in §2.2.2. The eigenstates are not consecutive, starting with the fourth in the upper left and ending with the 160th in the lower right. These are contour plots of coordinate space representations of the absolute squares of the eigenstates, and it is straightforward to count the nodal planes for the first several of these (up to $n=39$ or 46), and thus quantum numbers can be assigned to them. For example, the first state has two nodes and the second ($n=6$) three. Note that the nodal planes become distorted as energy is increased, even where they can be counted. The most important trend in figure 1 is the breakdown of the progression with increasing energy. At first this happens in a gradual manner ($n=46$–62), but then the eigenstates become complicated and it is difficult to discern any progression, though several of the complicated eigenstates are similar (73, 82, 92 and 117 as well as the pair 129 and 160).

It might seem strange to show such a complicated set of plots as figure 1, but I want to give a flavour for the complexity of the eigenstates of such a simple system, and also to set the tone for the rest of the paper. The first 12 panels of figure 1 show a pattern that breaks down in the last eight panels, where the eigenstates become complicated. The realization of the goals noted in the abstract depends on the discovery of such patterns, the understanding of their existence, and the extraction of useful information from complicated data, even when there are no apparent patterns. In this regard, the set of eigenstates presented in figure 1 were extracted via the hierarchical analysis of §3.2 as applied in §4.1 (see the discussions of figures 37 and 38).

0144–235X/95 $10·00

2. Discussion

2.1. *Review*

This section contains the major part of the review of the literature, although there are many citations to other work in the rest of the text. The survey of other work is not exhaustive, and I apologize ahead of time for slighting anyone. One of the reasons for avoiding an extensive review is that a broad survey of the field relevant to the present work has appeared recently (Uzer 1991).

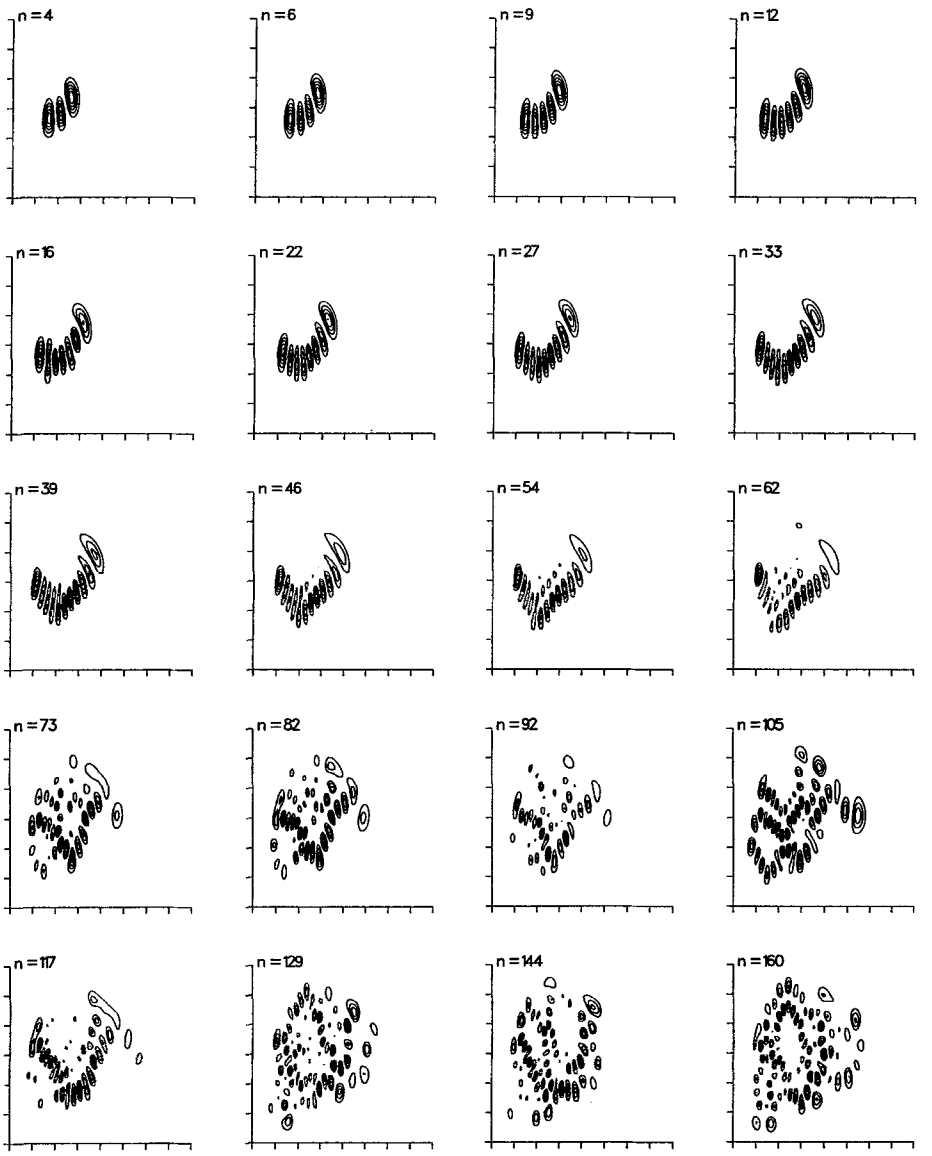

Figure 1. A series of eigenstates for system (2) of § 2.2.2. These have the same axes limits as the rest of the figures for this system (see figure 18 for axes labels). The headings indicate state number.

There are several areas which may be reviewed to put the present work in a broader context and three are chosen which are related to the study of intramolecular energy transfer in bound or metastable molecules: (1) models of intramolecular vibrational redistribution (IVR), (2) analysis of spectra and eigenstates, and (3) the classical–quantum correspondence.

2.1.1. *Models of IVR*

A common method of modelling IVR pictures the process originating from the couplings of manifolds of states. In the simplest versions of this approach, which were developed to understand spectroscopic experiments and originated in the radiationless transition literature (Jortner *et al.* 1969, Freed 1976, Uzer 1991), a non-stationary state (called 'bright' state) is excited via some sort of photo-excitation process. Since it is not an eigenstate it will 'decay' (i.e. intramolecular energy transfer will take place). This is generally assumed to be due to the mixing of vibrational eigenstates, which can mix due to anharmonic couplings or coupling with rotations. The decay from the bright states occurs into a bath of 'dark' states which are often taken to be the eigenstates of the system. There are many recent papers discussing models of IVR within this general approach that have appeared since the survey by Uzer (1991), see, for example, Pate *et al.* (1991), Jonas *et al.* (1993), Perry (1993).

Another way of modelling intramolecular energy transfer is less common and has its roots in the unimolecular reaction literature (Robinson and Holbrook 1972, Forst 1973, Hase 1976) and we refer the reader to several articles in this area (Bunker and Hase 1973, Marcus *et al.* 1984, Davis 1985), with Uzer (1991) also providing a review. This approach is rooted in classical mechanics, and it models intramolecular energy transfer as the flow between various regions of phase space separated by intramolecular bottlenecks. A rigorous way to define bottlenecks for systems with two degrees of freedom has been developed in the nonlinear dynamics literature (MacKay *et al.* 1984, 1987), and it has been applied to intramolecular dynamics (Davis 1985, 1988, Davis and Skodje 1992). This approach will be an explicit or implicit part of the comments in the rest of the paper. The hierarchical analysis described below also fits well into the model discussed in the previous paragraph.

2.1.2. *Analysis of spectra and eigenstates*

The most common spectroscopic methods (Califano 1976, Hollas 1982, Papousek and Aliev 1982, Gordy and Cook 1984) are not discussed, because our main interests lie in spectra and eigenstates of highly excited systems, where these procedures tend to break down. One approach is statistical, and was developed in the nuclear physics literature (Brody *et al.* 1981). It relies on the premise that the spectroscopy of highly excited systems is so complicated that the best one can do is statistical analysis. Statistical approaches have been used many times in the chemistry literature to analyse energy levels (Haller *et al.* 1983, Lehmann and Coy 1987, 1988, Persch *et al.* 1988, Chen *et al.* 1990, Hamilton 1990, Delon *et al.* 1991, Karrlein 1991), intensities (Levine 1988), and eigenstates (Burleigh and Sibert 1993).

The statistical approaches have a couple of very useful features. First, they are based on well defined mathematical models and universal properties have been derived for the level statistics and intensity fluctuations of various limiting cases. Second, and related, is that it is possible to condense a large amount of information with a few parameters based on the universality of distributions. A drawback is that the methods may discard useful information, because they rely on statistics.

A second approach starts with the observation that even when spectra of highly excited molecules are complicated, lower resolution versions of them might be simple (Pique 1990). Characteristics of smoothed spectra have been associated with the classical motions of molecules (Gomez Llorente *et al.* 1990). It has been possible to assign smooth features (Yamanouchi *et al.* 1990, 1991), and to use this as an aid for understanding IVR processes (Jonas *et al.* 1993). A procedure for estimating 'quantum chaos' is based on studying spectra as resolution is changed (Heller 1980).

There are two drawbacks to previous work on the smoothing of spectra: only a few levels of resolution have been probed and the smoothing has not been done in a systematic manner. The hierarchical analysis developed in Davis (1993) addresses these two drawbacks, providing a systematic procedure for studying smoothed spectra at all levels of resolution. Although the hierarchical analysis was originally developed to analyse experimental spectra, it provides a procedure to study energy transfer in detail if a theoretical model of the spectrum based on the eigenstates is available. This is done via the generation of 'smoothed states' (§ 3.2), which are associated with smoothed spectral features, as described in Davis (1992) (see also, Gomez Llorente *et al.* 1992), with a time-dependent procedure outlined earlier by Imre and co-workers (Zhang and Imre 1989, Tang *et al.* 1991) (see also Sadeghi and Skodje 1993). The use of the hierarchical analysis in conjunction with the smoothed states is related to the two approaches to IVR noted above. For example, the smoothed states at a given level of resolution might be thought of as 'bright' states compared to higher resolution 'dark' states.

2.1.3. *Classical-quantum correspondence for highly excited systems*

There is a good understanding of the correspondence between classical and quantum dynamics for systems which are not highly excited, that is where the dynamics is quasiperiodic. The success of semi-classical quantization attests to this (Noid *et al.* 1981, Ezra *et al.* 1987). There are quantum effects in quasi-periodic regions of phase space, for example tunnelling (Davis and Heller 1981), but these are well understood. The situation is different when the classical dynamics is chaotic. There has been some progress on systems whose dynamics is so chaotic that there is no regular motion whatsoever (hyperbolic systems, see, for example, Gutzwiller 1990, and Gaspard and Rice 1989a-c). However, the relationship between the classical and quantum dynamics is not well understood when the dynamics is not hyperbolic. There are several recent books and review articles which address the relationship between classical and quantum dynamics for chaotic systems (Stechel and Heller 1984, Giannoni *et al.* 1991, Haake 1991, Reichl 1992).

The approach presented here is a bit different than much of what is included in the above references, and it is outlined in previous papers (Davis 1988, Davis *et al.* 1991). One of the differences is that it is based on understanding the correspondence in terms of perturbations (possibly very strong) on regular motion. This seems useful, because of the tradition in chemistry for classifying states, and eigenstates can be classified when the dynamics is regular (see above). It has been asserted (Gutzwiller 1988) that it is better to think of systems which are weakly chaotic (this includes most bound molecular systems), as perturbations on the hyperbolic limit. This may be a reasonable way to think about the classical dynamics, but quantum mechanics poses a different challenge. Consider the stadium billiard, which is an example of a system with no regular motion. It has been known for several years that its low-lying eigenstates appear regular (Shapiro *et al.* 1984, Bai *et al.* 1985). At

the same time, there are mathematical theorems (Schnirlman 1974, Colin de Verdiere, 1985, Zelditch 1987) which state that asymptotically (with energy) most eigenstates are evenly spread over the energy shell in a coarse grained sense. The question remains as to the nature of the eigenstates between the two limits, and because low-energy eigenstates are simple it seems reasonable that states at intermediate energies might be understood in simple terms. The methods outlined in this paper can be used to extract information about the classical-quantum correspondence for such classically chaotic systems and provide information about the nature of their eigenstates.

2.2. *Systems studied*

A brief review of the systems studied in this paper is presented. Although the first three systems are only two degrees of freedom, their dynamics can be complicated at high energy, and the study of them provides evidence for the usefulness of the analyses described below.

2.2.1. *System (1)*

It consists of the following Hamiltonian:

$$H=\frac{1}{2}(p_x^2+p_y^2)+\frac{1}{2}(\omega_x^2x^2+\omega_y^2y^2)+\lambda x^2y, \tag{1}$$

where $\omega_x=1{\cdot}1$, $\omega_y=1{\cdot}0$, and $\lambda=-0{\cdot}11$, with $\hbar$ set to $1{\cdot}0$ in the quantum and semiclassical calculations. The dissociation energy is $15{\cdot}125$. If has been studied several times in the past (Heller *et al.* 1980, Davis and Heller 1981, Davis 1988), and a modified version has been used to model a spectrum of benzophenone (Frederick *et al.* 1988). This system is of interest because it has a well defined quantum effect (Davis and Heller 1981), tunnelling between local mode doublets, and this can be used to gauge the degree of classical-quantum correspondence. The level of chaos exhibited in this system is weaker than the next two, but is probably more similar to realistic molecular systems.

2.2.2. *System (2)*

It consists of the following Hamiltonian:

$$H=\frac{1}{2}(p_x^2+p_y^2)+V(x,y) \tag{2}$$

$$V(x,y)=\frac{1}{2}\omega_y^2y^2+D_e\{1-\exp[-\alpha(x-\gamma y)]\}^2-D_e, \tag{3}$$

$\omega_y=0{\cdot}0059$, $D_e=0{\cdot}088$, $\alpha=0{\cdot}01049$ and $\gamma=0{\cdot}5$, with all constants being au. It has been studied previously (Davis *et al.* 1982, Gibson 1987, Davis 1992, 1994a, b). At low energy the dynamics is regular, but there is widespread chaos by $E=-0{\cdot}048$, and what appears to be complete chaos at $E=-0{\cdot}008$.

2.2.3. *Oval billiard*

This system is a one-parameter family of two-dimensional enclosures. The control parameter is δ. At $\delta=0{\cdot}0$ the billiard has the shape of the well known stadium. At $\delta=0{\cdot}66325$ it has the shape of a circle. There have been two studies of the classical dynamics of the oval billiard (Benettin and Strelcyn 1978, Henon and

Wisdom 1983) and many studies of the classical and quantum dynamics of the stadium (for example, Bunimovich 1974, McDonald and Kaufman 1979, 1988, McDonald 1983, Taylor and Brumer 1983, Heller 1984, 1991, Shapiro and Goelman 1984, Shapiro *et al.* 1984, Bai *et al.* 1985, Christoffel and Brumer 1986, Feingold *et al.* 1990, Meiss 1992). There has been one previous study of the quantum mechanics of the oval billiard (Davis *et al.* 1991). Although the oval billiard is not related to any molecular system, it is a very useful system to study because there has been so much work done on the dynamics of the stadium.

2.2.4. *$OCHI^-$ photodetachment spectrum*

This is the most realistic molecular system we have studied so far (Davis *et al.* 1994), with preliminary work also having been done on the intramolecular dynamics of HO_2 (Gazdy and Bowman 1992). The hierarchical analysis of $OHCl^-$ follows several previous theoretical studies of this system (Koizumi and Schatz 1989, 1990, Koizumi *et al.* 1991). This case is reviewed here to demonstrate that it is straightforward to apply the hierarchical analysis to a calculation of this type.

2.3. *Motivation*

Figure 2 shows a series of wavefunctions. The top left state is an eigenstate of a two-dimensional harmonic oscillator and the quantum numbers (3, 8) can be assigned by counting the nodes, with the first number referring to quanta along the x-direction. The next three states in figure 2 were generated for system (2). They are not eigenstates, but what we refer to as 'smoothed states', which will be described in §3.2.

The next three states are ordered by complexity. The first (top right) is approximately an overtone in Cartesian coordinates and can be assigned as (0, 10). This is approximate because the state is distorted from an overtone in its nodal

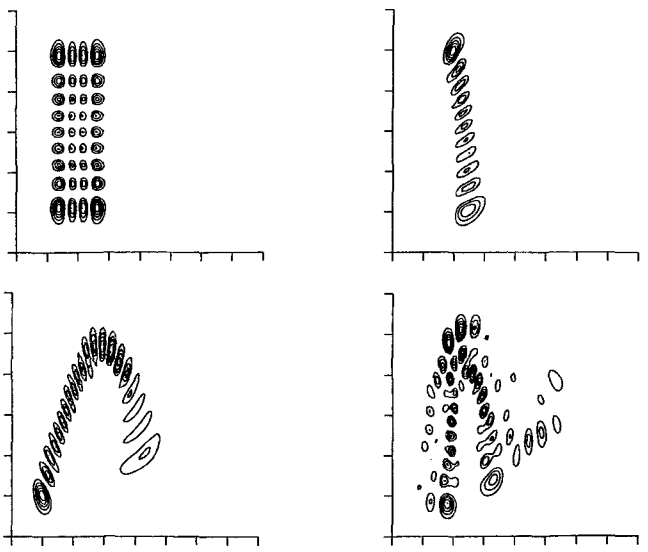

Figure 2. States demonstrating some of the complexities which can be encountered in strongly coupled systems.

pattern and density build up, although a projection onto an appropriate harmonic oscillator basis set would indicate one dominant basis state (0, 10). The second state of this group (bottom left) is a bit more problematical. There are 20 nodes along a path which is approximately parabolic, but this case differs from the first in that no single term in an harmonic oscillator expansion would dominate. However, the shape of the state is the result of a 2:1 Fermi resonance (for example, Noid *et al.* 1979), and an inspection of its expansion coefficients should reveal this. A group of basis states which form a polyad (Kellman 1994) will carry most of the oscillator strength with the state, although it will show some overlap with many other states due to distortions in its shape and density build up.

The last state in figure 2 (bottom right) presents two problems. Once again, an appropriate coordinate system may be difficult to define, although its shape is similar to the one on its left. The second problem appears more severe: it is difficult to assign a set of quantum numbers. One might wonder if it is part of a progression or is unassignable, and this will be addressed in § 3.2. On the other hand it is difficult to imagine that this state corresponds to a statistical distribution, because it is relatively simple.

Figure 3 shows a series of eigenstates for system (2). Most of the eigenstates are more complicated than the smoothed states of figure 2 and it is more difficult to assign them, though there are similarities. For example, the 113th eigenstate resembles the second state of figure 2 and the 102nd, 111th, and 122nd eigenstates resemble the third state of figure 2. It is difficult to find a close resemblance between the last state of figure 2 and any of the eigenstates in figure 3, although some are similar ($n=99$).

Figure 3 demonstrates the complexity of eigenstates of highly excited systems whose classical dynamics is very chaotic. The ability to assign states of systems with as few as two degrees of freedom is hampered by such complexity, with a further example being the eigenstates of the stadium billiard in figure 4. Many of the states in figure 4 appear hopelessly complicated, although there are some relatively simple ones (for example, 265 oo in the fourth row). Other states show distinct localization patterns, something first observed by McDonald (1983), which led to the work by Heller (1984) on what he called 'scars of periodic orbits'.

One of the goals of the work discussed here is the assignment of eigenstates like those in figures 3 and 4 in a manner similar to the first three states of figure 2. If this is not possible, then it would be useful to assign approximate quantum numbers, or to describe in a straightforward manner the energy transfer processes which cause the breakdown of assignments. Related to this point is another goal of the work: the nature of the classical–quantum correspondence for highly excited systems. For example, we have extended semi-classical quantization (Ozorio de Almeida 1988, Tabor 1989) into the chaotic region of phase space (Davis 1988). The extension was motivated by results like those presented in figures 5 and 6.

Figure 5 shows a surface of section (Lichtenberg and Lieberman 1992) at the top left, followed by a series of eigenstates which are near it in energy. The scatter of points on the surface of section is for a single chaotic trajectory which explores a large fraction of the available phase space. Even though a single trajectory fills a large region, the eigenstates are rather simple. Phase space transforms of these states demonstrate that they are localized in phase space in the region of the trajectory at the top left of the figure, and they are all distinct, contrary to what might be expected from the trajectory.

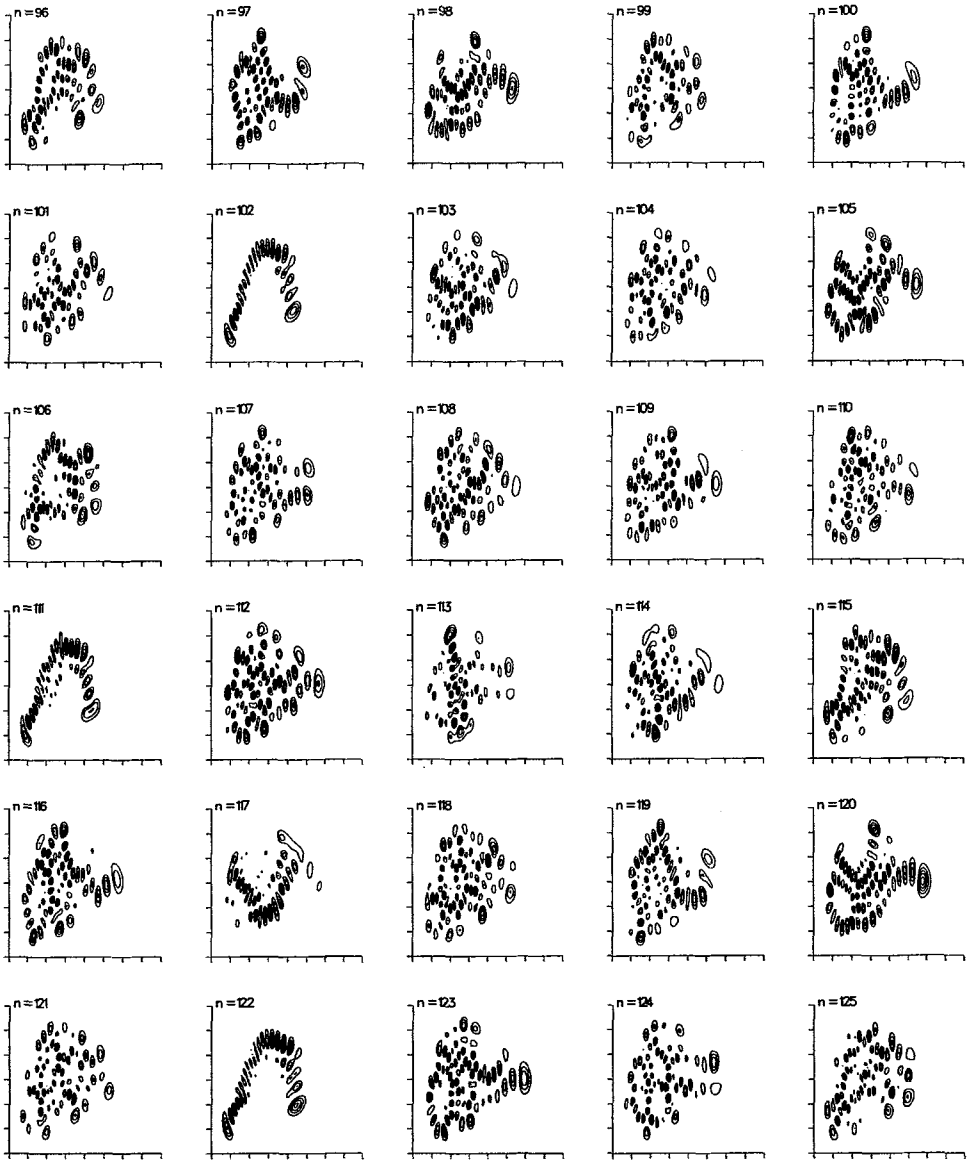

Figure 3. Consecutive eigenstates for system (2) from $n=96$ to 125.

The first three eigenstates in figure 5 are all halves of local mode doublets (Child and Halonen 1984). This case is interesting because an observable quantity reflects the classical-quantum differences observed in figure 5. Figure 6 shows a series of local mode doublet splittings. Such splittings are attributed to dynamical tunnelling (Davis and Heller 1981), which is normally expected when there are no classical trajectories connecting two equivalent types of classical motion, which are always coupled quantum mechanically because of symmetry. The splitting between the doublets goes down the farther apart in phase space the equivalent classical motions

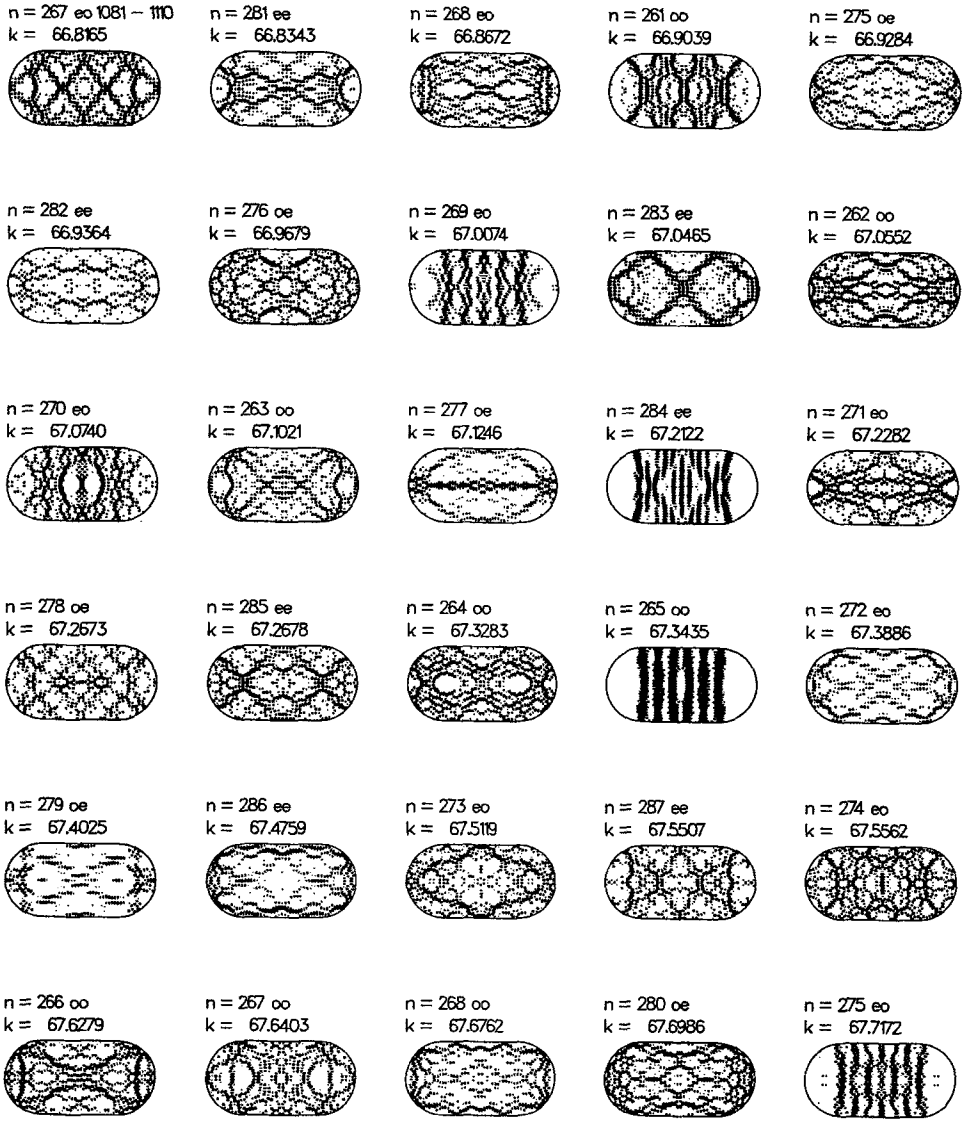

Figure 4. Eigenstates of the stadium billiard (§2.2.3.). They are labelled by $k(E=k^2/2)$ and the state number for their particular symmetry. There are two lines of symmetry in the stadium and the labels are ee, eo, oe, and oo with the first letter referring to even or odd with respect to reflection through the y-axis and the other label for the x-axis. In terms of all the symmetries, the eigenstates start at 1081 in the upper left and end at 1110 in the lower right.

are, and thus one would expect that splittings would decrease as energy is increased if there were no classical trajectories connecting the equivalent motions. Figure 6 shows examples of splittings which decrease with energy, but the classical chaos in figure 5 is widespread and classical trajectories can move between regions (figures 10 and 11). The small splittings are consistent with the localized eigenstates of figure 5,

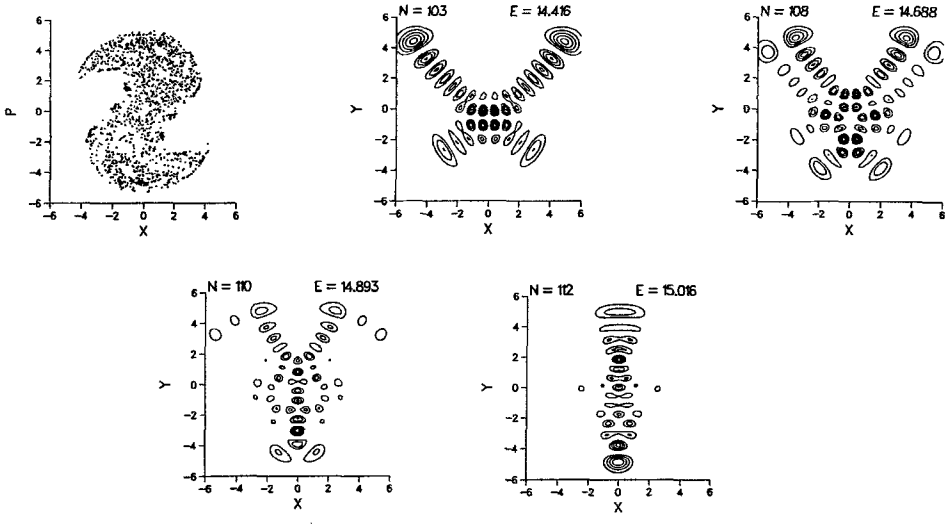

Figure 5. The top left plot shows a chaotic classical trajectory for system (1) at $E=15{\cdot}0$. Included with the trajectory are four eigenstates which occupy this region of phase space, based on an inspection of their phase space transforms.

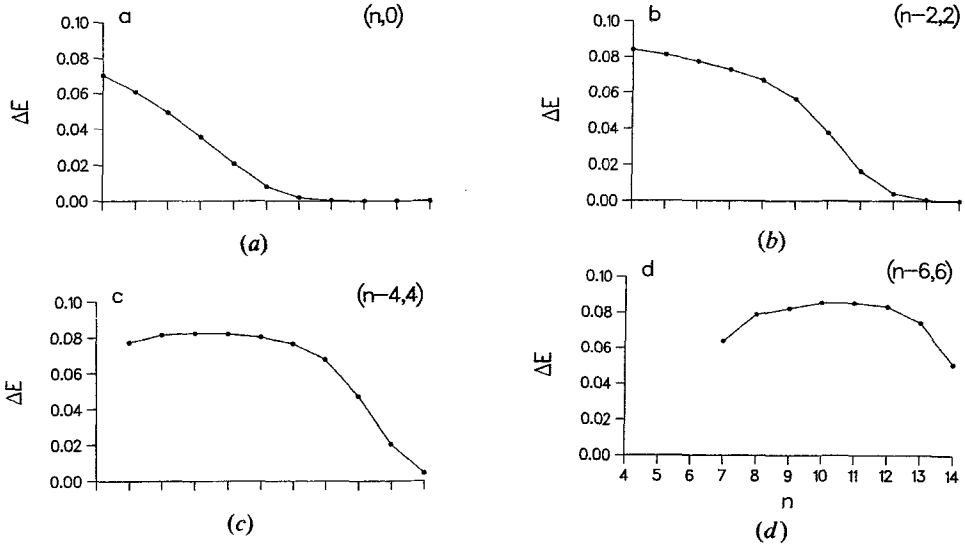

Figure 6. A series of splittings between adjacent states. At high energy the splittings become small, indicating the onset of local mode doublets. See the accompanying text and §3.1. for further details.

but inconsistent with the expectation of larger splittings when regions are connected by classical trajectories. It appears that the major route between the local modes is still tunnelling at high energy, even though there are classical trajectory pathways between them.

Another goal of the work is the extraction of information concerning intramolecular energy transfer time scales and pathways from the eigenstates of a variational

calculation. Although intramolecular energy flow is a time-dependent process and it seems natural to investigate it with wavepacket dynamics, figure 7 demonstrates the difficulty in extracting useful information directly from such a calculation. Figure 7 shows that the wavepacket looks simple up through the fourth panel (4461·7 atu, approximately 2·8 periods of the lower frequency normal mode), but gets complicated after that. The fifth and sixth panels are at 6606·6 atu (4·1 periods) and 8815·6 atu (5·5 periods) respectively, and their complexity demonstrates that a time-dependent calculation may be difficult to interpret. On the other hand, the eigenstates of figure 3 are also complicated. The hierarchical analysis described in § 3.2 provides information which lies between the two limits illustrated in figure 3 and 7.

This last point is emphasized in figure 8. The top plot shows a hierarchical tree resolved from a piece of the spectrum of the wavepacket in figure 7. The tree can be generated by convoluting the spectrum with windows of ever decreasing width (bottom left in figure 8) or by examining the Fourier transform of the convolution of a correlation function (lower right) with time windows of ever increasing width. Thus the tree can be used to study dynamics at ever increasing times, simply by going down the tree. Also, one can 'divide and conquer' a spectrum by studying it in different energy ranges chosen from selective cuts of a tree. For example, the tree in figure 8 can be split into two pieces by making a cut above its second highest node (see § 3.2). These two operations—following dynamics down a tree and investigating dynamics for selective cuts of a tree—provide the time and energy decompositions noted in the previous paragraph.

3. Types of analyses

3.1. *Semiclassical analysis*

Figure 9 presents a local mode doublet on the left. These eigenstates correspond to the point $n=11$ in figure 6(*b*) (the headings of the plots in figure 6 show normal

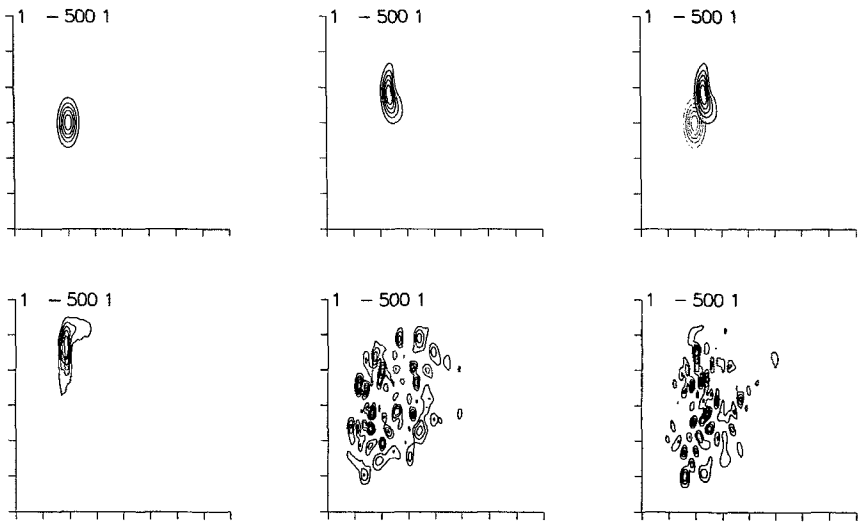

Figure 7. Time snapshots of a wavepacket moving in system (2). In the third panel of the top row the initial wavepacket (dotted contours) of the first panel is superimposed on the time evolved packet from the second panel.

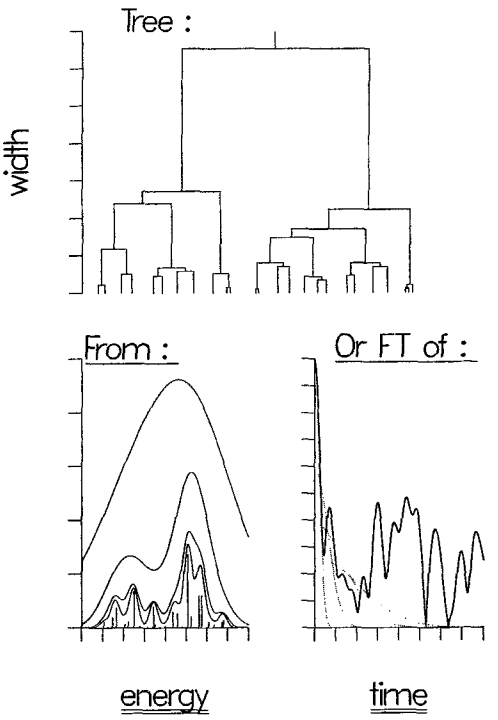

Figure 8. Using the hierarchical analysis of § 3.2., information similar to that shown in figures 3, 4 and 7 can be processed. A tree generated from the analysis is shown in the top of the figure, and two ways of generating it are shown below it.

mode quantum numbers (Davis 1988). Note the small splitting of these two states, with the headings indicating that the energies are equal to three decimal places. The local mode nature of these states is evident from linear combinations, presented on the right in figure 9. The eigenstates and wavefunctions in figure 9 are another example, along with the eigenstates in figure 5, of the apparent lack of any manifestation of classical chaos on the quantum eigenstates, a result noted previously (Weissman and Jortner 1982) for another, similar system. Even though there is chaos and the two local modes can communicate classically, the major route between the wavefunctions appears to be tunnelling, evident in the localization of the eigenstates and the small splitting.

The nature of the classical communication between the local modes is demonstrated in figure 10, which shows coordinate space plots of a trajectory at the same energy as the eigenstates of figure 9. These plots show time slices of a single trajectory, which moves from one local mode in figure 10 (*a*) to the other in figure 10 (*c*) by becoming normal mode-like in figure 10 (*b*). Figure 10 (*a*) and (*c*) can be compared to the local mode wavefunctions in figure 9, which have similar shapes.

The local-normal classical transition is investigated further with a surface of section for the trajectory of figure 10. Figure 11 (*a*) shows the complete trajectory and figure 11 (*b*)-(*f*) show consecutive time slices of it. Figure 11 (*b*), (*c*) and (*f*) show the same time slices as figure 10 (*a*)-(*c*). Figures 11 (*b*)-(*f*) also include a solid,

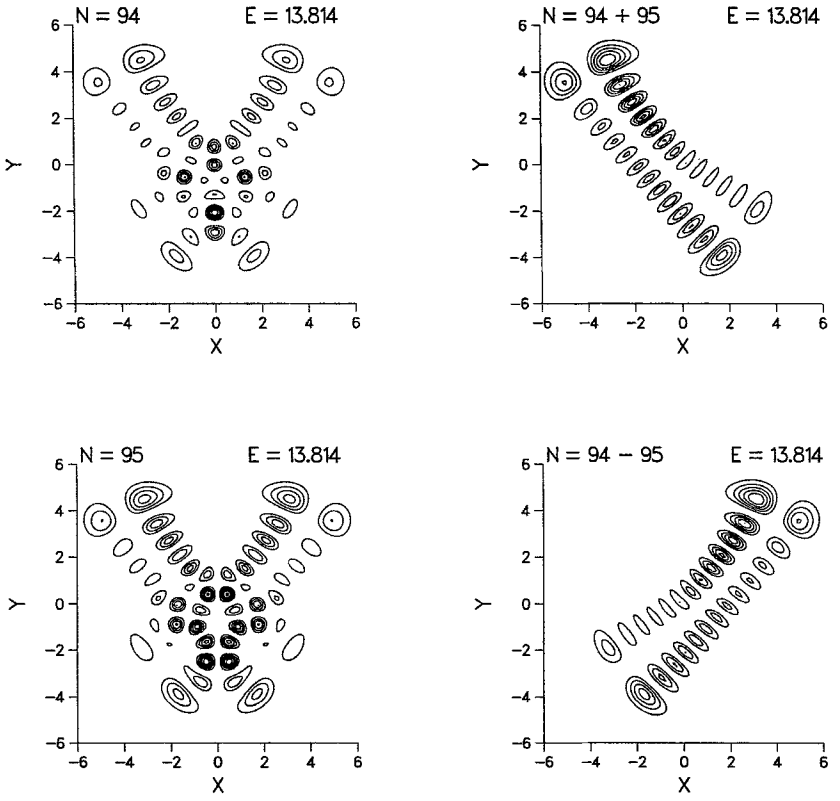

Figure 9. A local mode doublet for system (1) is on the left and linear combinations of the two states are on the right.

figure eight shaped curve which is a what is known as a broken-up separatrix. This curve is a generalization to the chaotic region of the well known concept of integrable separatrix (Guckenheimer and Holmes 1983, Lichtenberg and Lieberman 1992). The term 'broken-up' indicates that, unlike an integrable separatrix, trajectories can move across the curve from either the inside or outside. If the separatrix was integrable, no trajectories could behave like the one in figure 11. The degree of break up can be made more precise by calculating the amount of flux that flows across the separatrix for each iteration of the surface of section.

Figure 6 showed that the number of small spacings increases with energy, which is evidence for an increase in the number of local mode states. The key to understanding this from a semiclassical perspective depends on the broken-up separatrix plotted in figure 11. The size of the region enclosed by the separatrix increases with energy, as demonstrated in figure 12, with figure 13 (*a*) plotting the size against energy. Figure 13 (*a*) also includes dashed lines which indicate the Einstein–Brillouin–Keller (EBK) quantization conditions (Ezra *et al.* 1987) needed to support one (lowest curve) to four (highest) local mode doublets. At the energy of the states in figure 5, there is enough area to support three local mode doublets, in agreement with the quantum results presented there.

The previous discussion rationalizes the presence of a certain number of local mode doublets. However, figures 5 and 11 show that trajectories move between the

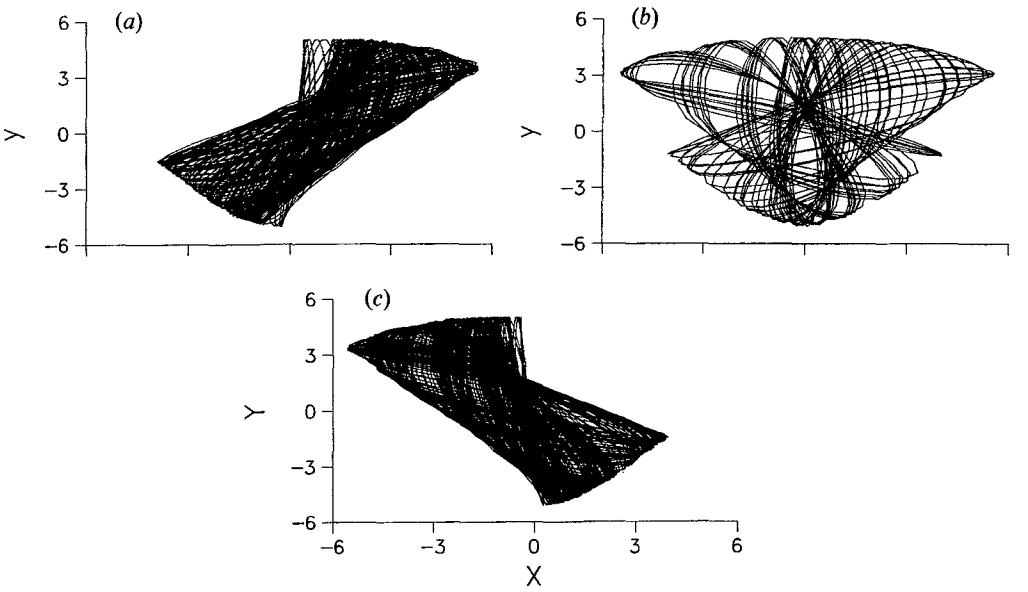

Figure 10. Pieces of a chaotic trajectory. In (*a*) the trajectory is in one local mode and in (*c*) it is in the other, symmetrically related one. Between these two it exhibits normal mode behaviour (*b*).

two halves of the separatrix, while quantum flow occurs via tunnelling. The semiclassical rationalization for this discrepancy is given in figure 13 (*b*), which shows the flux across the separatrix against energy. The flux is always smaller than the amount of area needed to support a single quantum state, which is $\pi(\hbar = 1{\cdot}0)$, the quantizable action for a ground state, and this probably leads to the difference

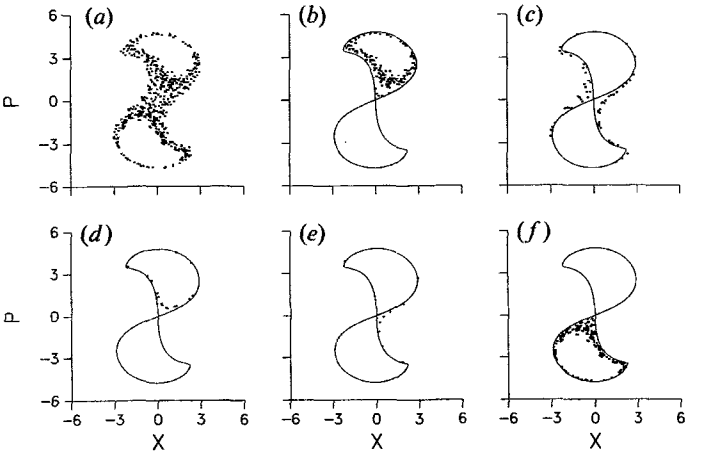

Figure 11. A surface of section for the trajectory from figure 10 in (*a*) and consecutive time slices of the trajectory in (*b*)–(*f*). The portions in (*b*), (*c*) and (*f*) correspond to figure 10 (*a*–*c*), in that order. The plots also include a broken-up separatrix which demarcates local mode motion (*b*, *d*, *f*) from the normal mode motion (*c* and *e*).

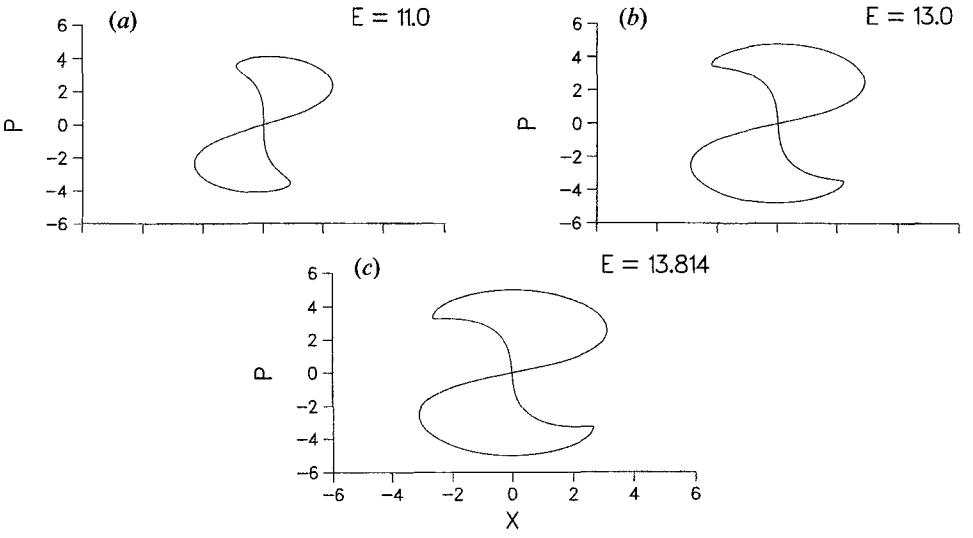

Figure 12. A broken-up separatrix at three energies, including the energy of the eigenstates in figure 9.

between the classical and quantum dynamics. Similar arguments have been made by others for different systems (Brown and Wyatt 1986a, b, Fisherman *et al.* 1986, Radons *et al.* 1986, 1989, Bohigas *et al.* 1993) where classical-quantum differences also occur. Further semiclassical analysis can be used to rationalize the localization of individual eigenstates (Davis 1988).

3.2. *Hierarchical analysis*

Our study of assignability and energy transfer starts with the generation of spectra formed from the overlap of wavepackets with the eigenstates of the system of study. The wavepackets are Gaussians:

$$g(x,y)=\exp[-\alpha_x(x-x_0)^2-\alpha_y(y-y_0)^2+ip_x(x-x_0)+ip_y(y-y_0)], \tag{4}$$

with $\alpha_x=0{\cdot}022$ and $\alpha_y=0{\cdot}0325$ for system (2). $G(x,y)$ has expectation values of positions (x_0, y_0) and momenta (p_x,p_y) which centres it in phase space. The wavepacket of figure 7 has the following values: $(x_0,y_0,p_x,p_y)=(0{\cdot}0,\ 0{\cdot}0,\ p_x(E),\ -0{\cdot}1)$, where $p_x(E)$ is adjusted so that expectation values of positions and momenta fix the centre of the wavepacket at a classical energy, here $E=-0{\cdot}028$.

The spectrum of the wavepacket of figure 7 is shown in the upper left of figure 14. Lower resolution versions of a middle portion are presented in panels *b*–*f*. The lower resolution versions were formed by convoluting it with a window function:

$$\Omega(E)=\sum I_k\Gamma(E,E_k) \tag{5}$$

where I_k, the intensity of the kth line, is:

$$I_k=|\langle g(x,y)|\Psi_k\rangle|^2, \tag{6}$$

and Ψ_k is the kth eigenstate of the system to be studied. Γ is chosen to be a Gaussian with the following form:

$$\Gamma(E,E_k)=\exp[-(E-E_k)^2/\sigma^2). \tag{7}$$

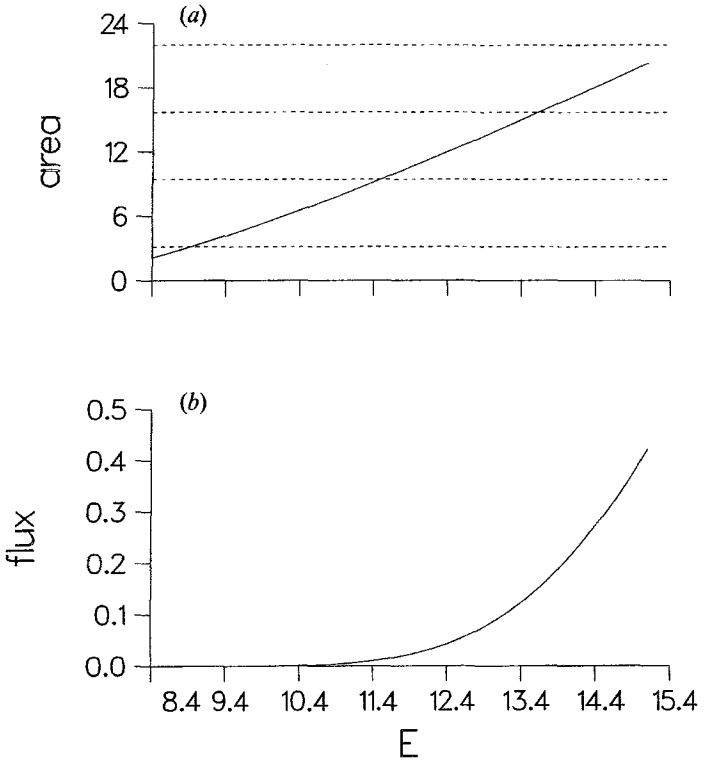

Figure 13. The top plot shows the area of the local-normal separatrix as a function of energy (solid line) plus dashed lines to indicate when the area is large enough to support a new quantum state based on semiclassical arguments. The dashed lines are for $n=0$-3. The bottom plot shows the flux across the separatrix against energy.

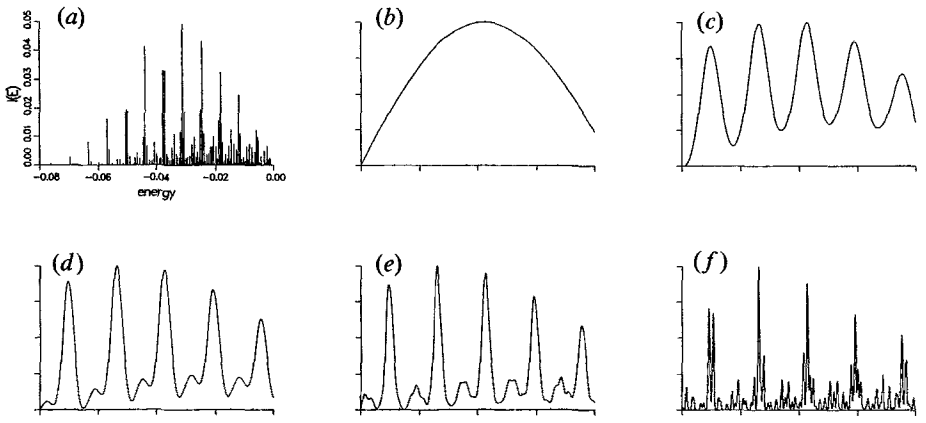

Figure 14. A stick spectrum for the wavepacket described in the text is shown in (*a*) and smoothed versions of the middle portion of the spectrum ($E=-0{\cdot}0412$ to $-0{\cdot}0103$) are shown in (*b*)-(*f*).

The utility of smoothing is demonstrated by comparing figure 14(*a*) with figure 14(*c*) and (*d*). The stick spectrum has a series of tall lines which, except for a pair of lines at $\sim -0{\cdot}038$, is monotonic. This might indicate a progression and the smoothed spectrum of figure 14(*c*) confirms it. A better example of the utility is the comparison of the stick spectrum with figure 14(*d*). Although the pattern of figure 14(*c*) might be anticipated from figure 14(*a*), it is more difficult to anticipate the series of small side peaks in figure 14(*d*).

The rationale for a hierarchical decomposition of a spectrum is provided by the last four panels of figure 14. Small peaks split off large peaks, suggesting a parent/child relationship among the peaks. By studying a spectrum as resolution is changed continuously, one can generate a genealogy of the lines, which can be visualized with a hierarchical tree, such as the one plotted in figure 15 for the spectrum of figure 14(*a*). This tree describes the way the spectrum evolves as resolution is changed. As peaks split off other peaks they form nodes on the tree. As one moves down the tree (i.e. resolution is increased or longer time-scales), more peaks are represented, with the number of peaks at a given level of resolution indicated by the number of vertical lines. The major features of the smoothed spectra of figure 14 are embodied in the tree. For example, the nodes starting at a width of 1·1 and descending to 0·7 describe a set of peaks, five of which are shown in figure 14(*c*). At higher resolution the side peaks of figure 14(*d*) are formed, and this is reflected in the set of nodes between 0·2 and 0·3.

A tree defines a genealogy for the lines of a spectrum. The distance between two lines is defined from the tree by the height of their most recent common ancestor. For example, the first and second lines of the spectrum are shown by the two vertical lines which descend at the bottom left of the tree in figure 15. These two lines meet at a width of 0·71, which defines the distance between the two. The matrix of all distances defines a relationship among all the lines of a spectrum, and this matrix is used for much of the statistical analysis described in Davis (1993) and applied in other places (Coy *et al.* 1994, Davis 1994a, b, Davis *et al.* 1994). We do not discuss the statistical analysis in this paper, and the interested reader is referred to these references.

Using the tree of figure 15, groups of states can be associated with spectral features. For example, lines 2–4 of the tree of figure 15 are part of a group, as are

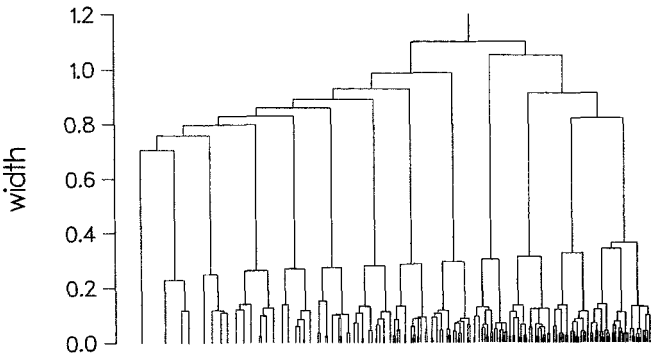

Figure 15. A hierarchical tree generated from the spectrum of figure 14(*a*). The *y*-axis has a scaled version of σ (equation 7). To convert width to σ, multiply by 0·00387.

lines 3–4, because they result from a single cut of the tree. Lines 2–3 are not a group. These groups of states are used to generate 'smoothed states', which help to assign smooth features of a spectrum. Smoothed states are defined as:

$$\Phi(x,y)=\sum_k c_k \Psi_k(x,y), \qquad k \in L, \tag{8}$$

where L refers to the Lth group of the tree. The c_k's are the overlaps of the eigenstates with the initial state which generates a spectrum, the arguments inside the absolute value in equation (6).

The group L in equation (8) is a subtree, because it results from a single cut of the tree. Figure 16 shows a series of subtrees extracted from the tree of figure 15 by making a cut all the way across the tree between 0·37 and 0·71. The subtrees in figure 16(*a*)–(*e*) correspond to the peaks of figure 14(*c*) from left to right. They describe the evolution of the spectrum in localized regions of energy. It is the systematic study of subtrees that leads to the notion of 'divide and conquer'.

In studying energy transfer properties of highly excited systems we investigate smoothed states at all levels of resolution. A good way to start such an investigation is the examination of those states formed from a set of subtrees generated with a cut of the tree between two widely spaced nodes. From our experience, such states are most likely to be assignable, because large gaps indicate differences in time-scales, bottlenecks to energy transfer, or a combination of both. The subtrees in figure 16 were chosen for this reason and the top row of figure 17 shows the smoothed states for these subtrees. The next two rows of figure 17 correspond to the peaks of figure 14(*d*), with the upper row of this pair representing the large peaks and the bottom the small peaks. The state labelled 107–120 in the middle row has previously been presented in figure 2. The states in figure 17 can be assigned a set of quantum numbers, thus assigning the peaks in figure 14(*c*) and (*d*). The first set in the top row is an overtone progression in a coordinate which is mostly along the y-axis. The next two rows indicate that the peak/sideband structure of figure 14(*d*) corresponds to a short overtone/combination sequence.

The plots in figure 17 demonstrate that the hierarchical analysis can aid in assigning smoothed features of the spectrum, even when it is not obvious from the

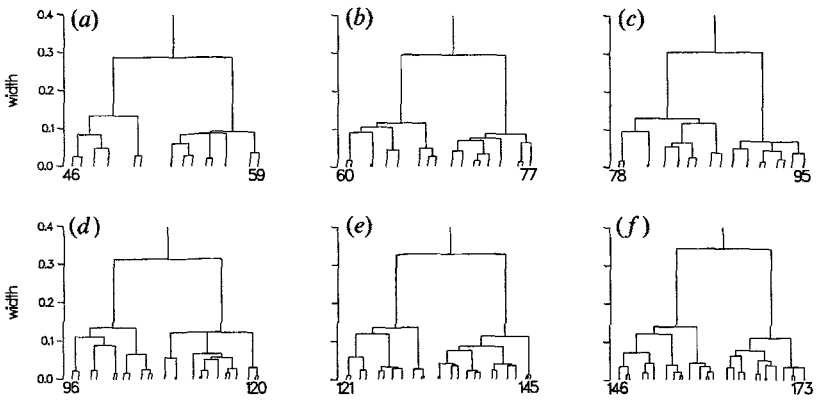

Figure 16. Subtrees from figure 15 formed by cutting all the way across between a width of 0·25 and 0·70.

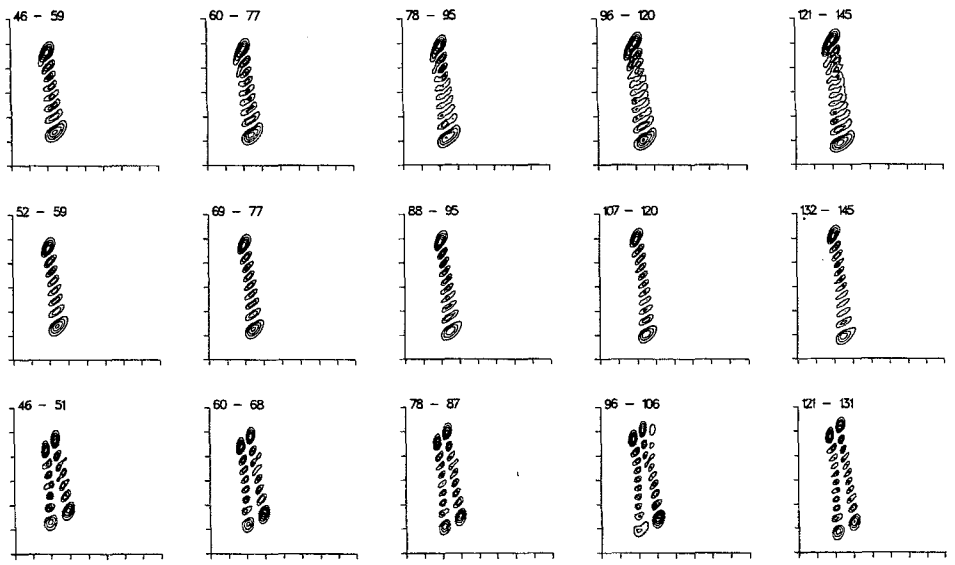

Figure 17. Smoothed states from equation (8). The groups of eigenstates are listed on each plot. The top row shows overtones generated from subtrees in figure 16(*a*–*e*). The bottom two rows show smoothed states for the groups made by cutting the subtrees in figure 16 above their second highest nodes.

fully resolved spectrum or the eigenstates (figure 3) that certain structures exist. This is emphasized in figure 18, which shows a series of eigenstates chosen from the hierarchical analysis, where they have been designated the parent line of a given peak. The eigenstates in the left column are parent lines of the large peaks in figure 14(*d*) and the eigenstates in the right column are the parent lines of the set of small peaks in figure 14(*d*). In the same way that it was difficult to observe the small peaks of figure 14(*d*) in figure 14(*a*), it is difficult to see a resemblance between the eigenstates in the right column of figure 18 and the smoothed states of the bottom row of figure 17. The eigenstates of the left column of figure 18 do resemble the smoothed states in the middle row of figure 17, but it is difficult to assign a set of quantum numbers to the eigenstates.

The main reason the eigenstates of figure 18 are difficult to assign is the complicated intramolecular energy transfer of system (2). Figure 19 illustrates energy transfer by presenting two of the smoothed states (solid lines) from figure 17 on top of their respective parent eigenstates from figure 18 (dotted lines). One can observe in figure 19 that wavefunction density has moved out from along the direction of the overtone. Such detail is not evident from examination of either the eigenstates (figure 3) or the wavepacket (figure 7).

The wavepacket of figure 7 has been used to generate results in two previous articles (Davis 1992, 1994a), because it yields simple plots of smoothed spectra (figure 14) and smoothed states (figure 17). However, system (2) has complicated dynamics, which led to the development of tools (Davis 1994b) to choose a set of wavepackets which would provide insight into the intramolecular dynamics of a system. These can yield interesting smoothed spectra and smoothed states, and figures 20–24 are presented to demonstrate this.

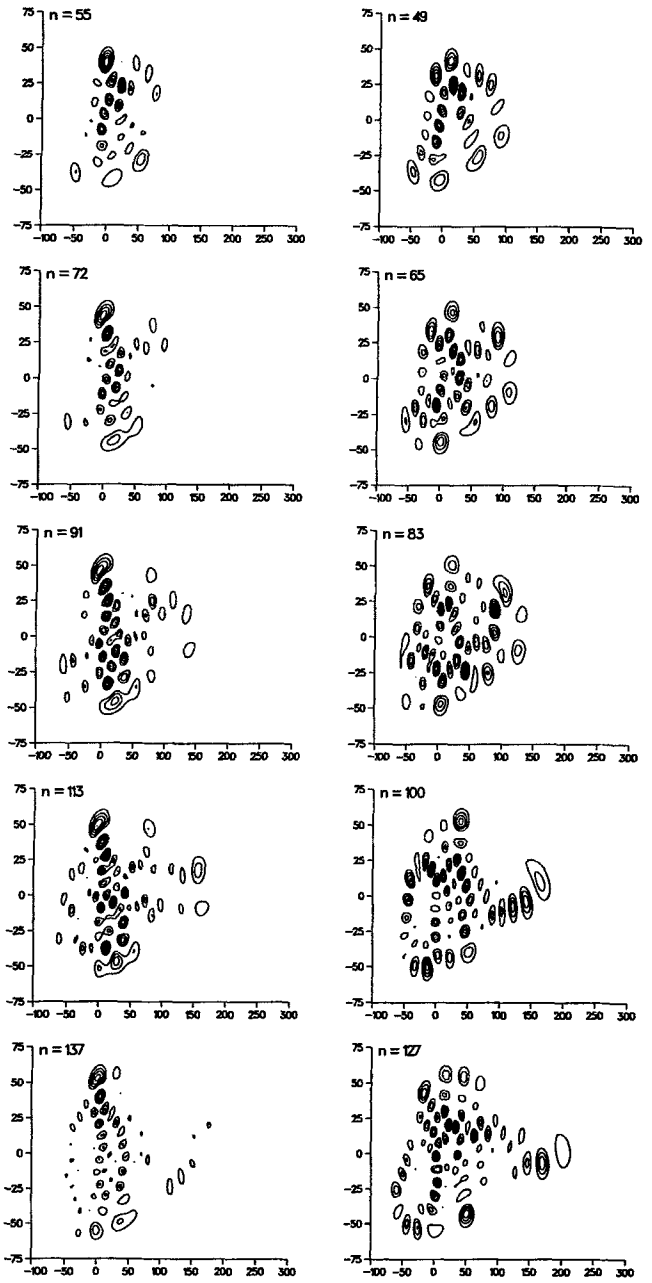

Figure 18. The eigenstates in the left column represent the parent lines of the smoothed states in the middle row of figure 17 and the eigenstates in the right column are the parents of the smoothed states in the bottom row of figure 17.

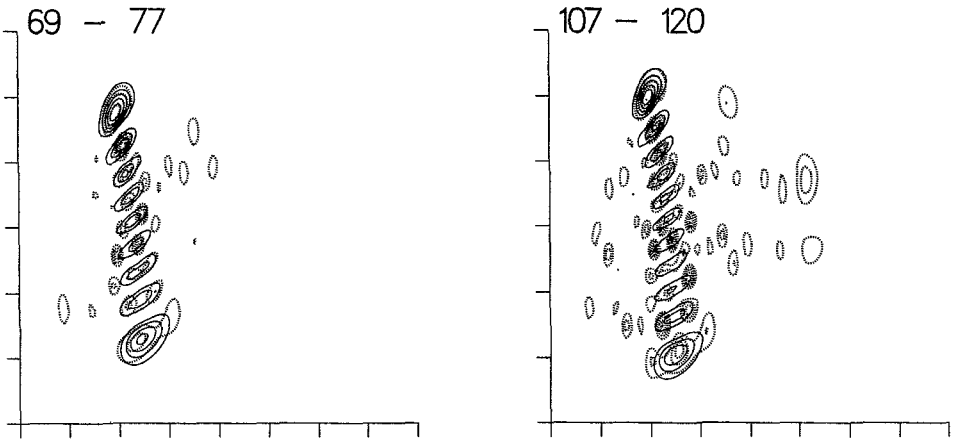

Figure 19. A comparison of two of the eigenstates ($n=72$ and $n=113$ see figure 18) (dotted contours) and two of the smoothed states.

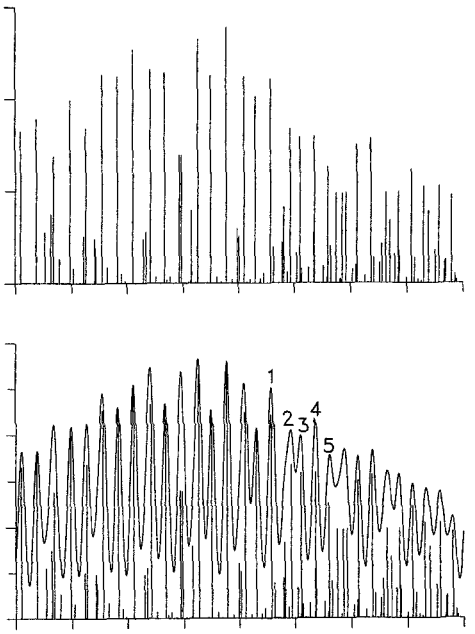

Figure 20. A portion of a spectrum for another wavepacket in system (2) is shown in the top plot and it is plotted again on the bottom plot, along with a smoothed version. The energy range of the spectrum is $-0{\cdot}0402$ to $-0{\cdot}00928$.

Figure 20 has a stick spectrum on the top for a wavepacket (equation 4) whose expectation values of positions and momenta are (0·0, 66·22, $p_x(E)$, 0·0465), with E, α_x, and α_y the same as the previous wavepacket. Unlike the spectrum of figure 14a, this one and smoothed verions of it (bottom plot) show no apparent regularity. Yet figure 21 shows smoothed states for peaks 1–5 and these are similar, evidence for a

progression, which can be assigned (Davis 1994b) once it is recognized they are distorted by a 5:3 classical resonance (Noid and Marcus 1986, Martens and Ezra 1987).

Figure 22 compares a set of eigenstates (left column) with smoothed states (right). The smoothed states were generated from a wavepacket at the same energy and with the same spread parameters as the previous two wavepackets, but it has different expectation values of positions and momenta: (0·0, −15·107, $p_x(E)$, 0·227). The state on the top right of figure 22 has already been presented in figure 2. Figure 22 again indicates how much easier it may be to assign smoothed states than eigenstates.

A more complicated example of assignability is presented in figure 23, which shows smoothed states generated from groups extracted from the subtrees of figure 16. Figure 16(*e*) and (*f*) indicate that there are distinct groupings for the combination halves of each of the subtrees. These are the left halves of the subtrees which yield combination states like those in the bottom row of figure 17. There are three groups of states embedded in the combination halves (for example 121-124, 125-128 and 129-131 in figure 16(*e*)). The subtrees in figure 16(*c*) and (*d*) do not have such good groupings (the differences in nodal heights are not as great), but three groups from the combination halves of these subtrees are also presented in figure 23. The states are arranged in figure 23 so that the smoothed states from each of the combination halves of the subtrees are plotted along rows and what appear to be progressions are plotted along columns. The second row does not have the states in numerical order, as do the others, because there is not a complete progression in the last column, with the last two states being the only members of the progression.

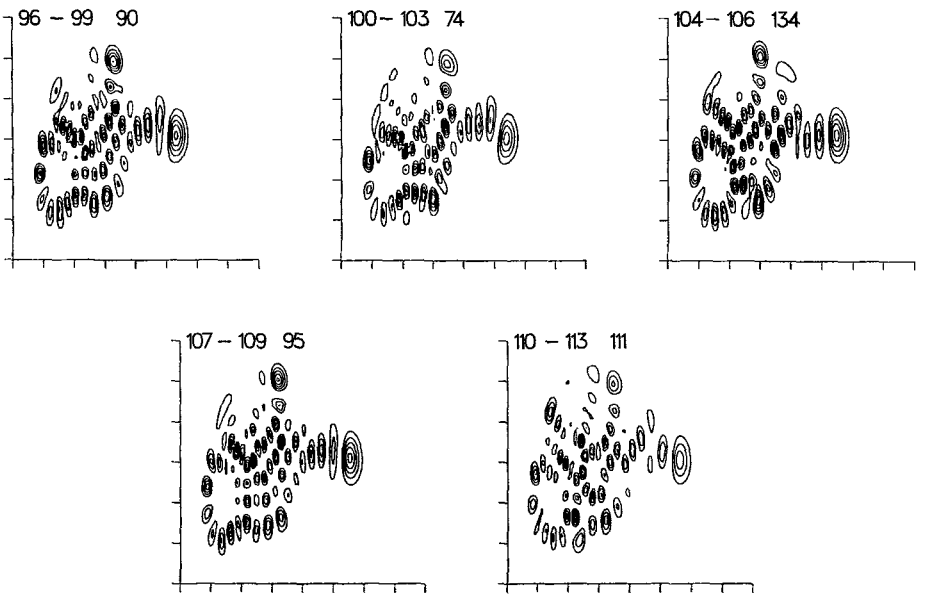

Figure 21. Smoothed states generated for the five numbered peaks in figure 20. The order of these is from left to right on the top and then left to right on the bottom corresponding to peaks 1–5 in figure 20.

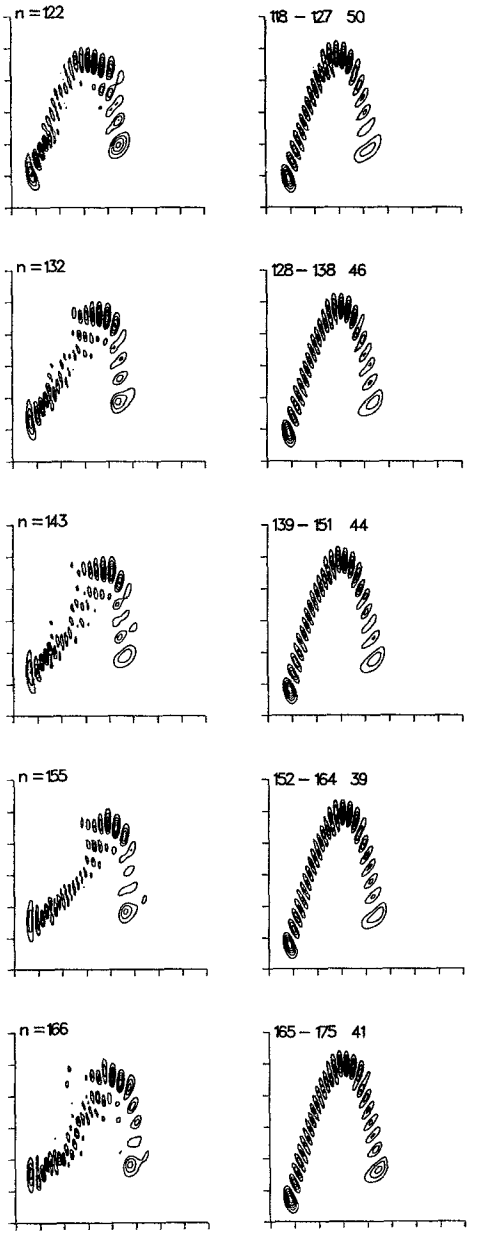

Figure 22. Another comparison between the eigenstates (left column) of system (2) and smoothed states.

Figure 23 shows evidence for progressions of states, based on the similarity of the plots in each column. This figure revisits the discussion of assignability for figure 2, because the 121–124 state in the first column, third row, was presented there. This state can be compared to the eigenstates $n = 121$–124 in figure 3, which are more complicated. An attempt to assign some of the states is made by seeking local nodal

patterns which simulate a 2:1 resonance, because, as noted in §2.3., the 121–124 state has the shape of a 2:1 resonant wavefunction. The picture of the state 121–124 indicates the nature of the attempt, by including a parabola and a straight line. These are coordinates used to examine cuts across the wavefunction, with similar cuts used for the other two states in the third row. The wavefunctions along these cuts are presented in figure 24. The top row of Figure 24 (*a–c*) shows cuts along

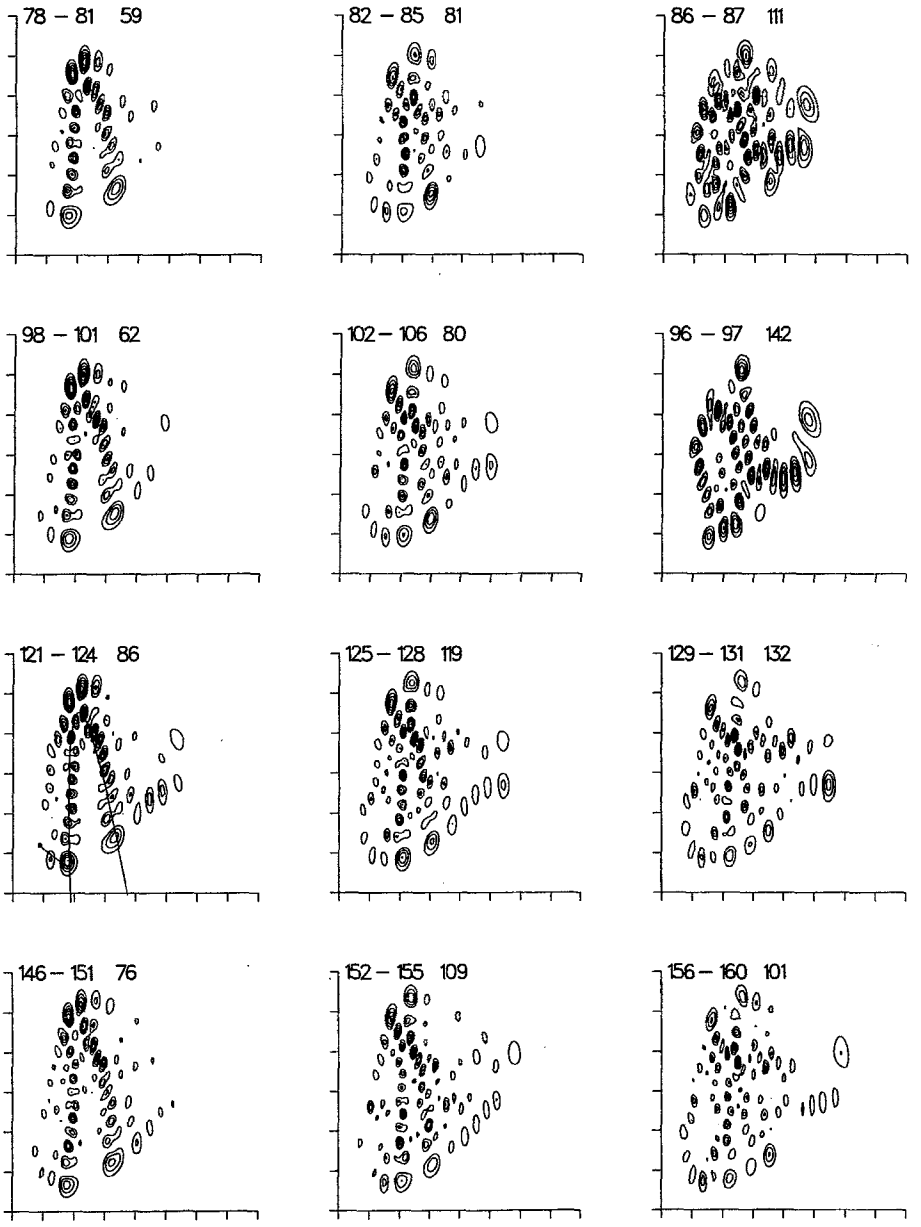

Figure 23. Smoothed states cut from the subtrees of figure 16.

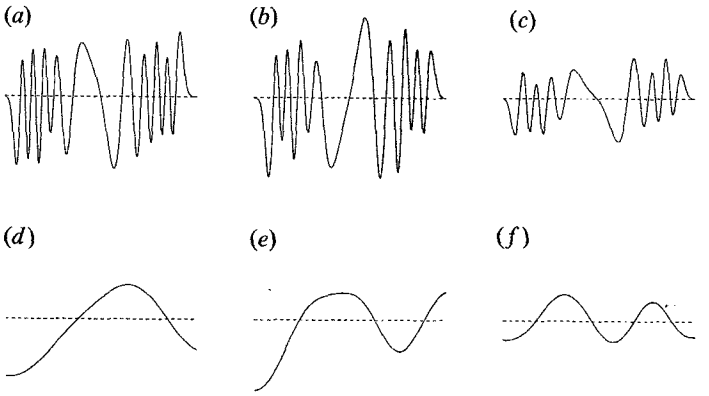

Figure 24. One-dimensional plots from the smoothed states in the third row of figure 23 along curves like those shown in the first state of row 3. The top row shows the wavefunctions along the parabolic paths and the second row along the straight lines.

parabolic paths and the second row shows cuts along straight lines. Moving from left to right, the nodes decrease by two in the top row (19, 17, 15) and increase by one in the bottom row (2, 3, 4), and this ratio is another indication of the resonant nature of the states.

Figure 23 is a good example of the usefulness of the divide and conquer aspect of the hierarchical analysis. This figure focuses on only a range of the spectrum, lines 78–160. This range was chosen because the hierarchical analysis pointed to interesting groupings in the subtrees of figure 16 (*e*) and (*f*). The analysis not only points to a range of the spectrum, but disconnected pieces of the range (78–87, 96–106, 121–131, 146–160), and this detail is difficult to observe without the hierarchical analysis.

Figure 19 demonstrated the utility of the hierarchical analysis for the study of energy transfer pathways by comparing smoothed states with eigenstates. However, it only showed two levels of resolution, and the hierarchical trees define several levels and many pathways between the smoothed states and the eigenstates. We have found it useful to study energy transfer pathways by following paths down trees, as is done in figure 25.

The top row of figure 25 shows two subtrees which were cut from trees generated from the spectra of two different wavepackets which are initially close to each other in system (2). The bottom four plots in each column of 25 show Husimi transforms (Husimi 1940) of smoothed states for the subtrees at the top of each column. The dots on each subtree indicate the paths taken down the subtrees which were used to discern groups of eigenstates summed to form smoothed states. The right column shows Husimi transforms of several states presented previously, the first two states in figure 17 and the last state in figure 23.

Figure 25 demonstrates the way energy transfer pathways can be mapped out using the hierarchical analysis. It also makes a point about sensitivity to initial conditions. While the wavepackets lie relatively close to each other initially and the Husimi transforms of the initial smoothed states are similar (second row), energy transfer pathways differ at later times. In the right column, a piece of the wavepacket moves into a region which is dominated by a 2 : 1 resonance (figure 22). In the left

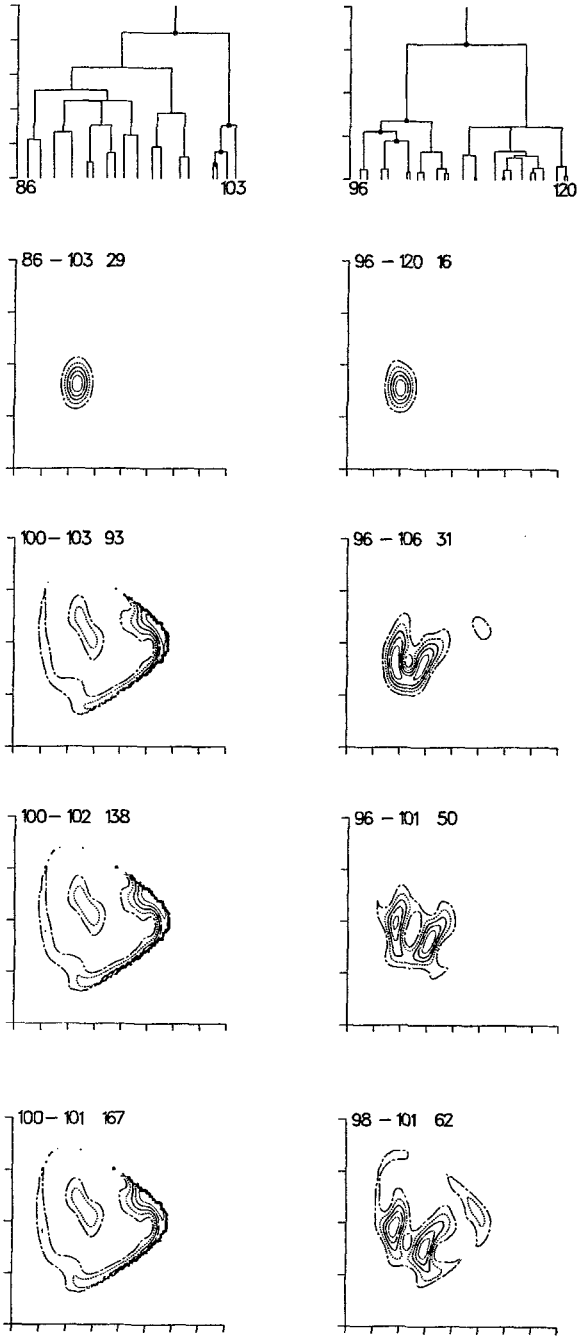

Figure 25. These plots show how different energy transfer pathways come into play for different initial wavepackets. The right column was generated for the wavepacket of figures 7, 14, and many other plots in the paper. The left column was generated by a wavepacket with the same parameters as the wavepacket in the right column, but with $(x_0, y_0, p_x, p_y) = (0{\cdot}0, 14{\cdot}74, p_x(E), -0{\cdot}093)$. The line types of the contours are ordered from lowest to highest in the following way: chain-dashed, dashed, solid, chain-dotted, dotted. The text has further details.

column, a smaller piece of that wavepacket moves into a different region, a 5:3 resonance (figure 21).

3.2.1. *Hierarchical analysis and correlation functions*

In this subsection we have not made an explicit connection with much of the work reviewed in § 2.1. Here we wish to make a connection with one type of spectral analysis. This approach (Gomez Llorente *et al.* (1990), Pique (1990)), and applications in many places (Delon *et al.* 1991)) starts with the Fourier transform of the spectrum (a correlation function; figure 7). The actual spectrum (including the intensities) or the energy spectrum (intensities assumed constant) is transformed. The transforms can be used to examine long-range correlations in a spectrum or can be used to associate its peaks with specific types of classical motion. We wish to point out how the hierarchical analysis can aid this approach.

Figure 26(*a*) shows a correlation function for the wavepacket of § 4.1. This function is the Fourier transform of the spectrum in figure 34(*a*). There are two or three distinct recurrences in the correlation function, but at later times there are no simple recurrences. Figure 26(*b*) shows the Fourier transform of a subtree of figure 35 (lines 1–59) and figure 26(*c*) shows another portion of the spectrum generated from two cuts of the tree (lines 60–124; figures 35–38). These portions were chosen based on the analysis of § 4.1., where it was noted there are distinct energy regions in the spectrum. The Fourier transforms in figure 26(*b*) and (*c*) are simpler than the one in figure 26(*a*), showing more distinct recurrences.

3.3. *Eigenstates of the oval billiard*

As noted in § 2.2., the oval billiard is a one-parameter family of two dimensional enclosures. At one value of the parameter ($\delta = 0{\cdot}0$) it is the completely chaotic

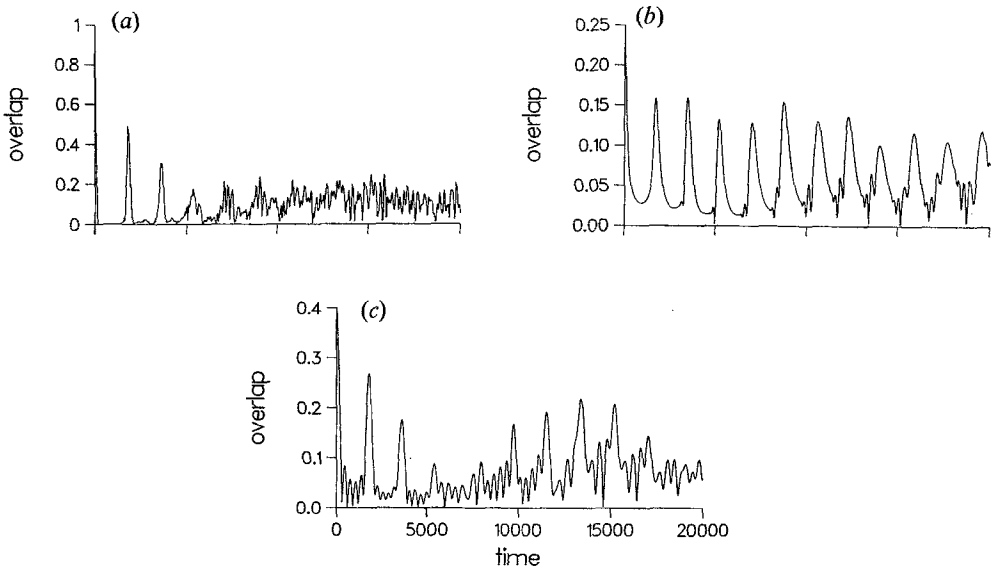

Figure 26. The top left plot is an autocorrelation function for the wavepacket of § 4.1. The other plots show autocorrelation functions for pieces of the spectrum of the wavepacket resolved from a hierarchical analysis.

stadium and at another value ($\delta = 0{\cdot}66325$) it is the integrable circle. Between these two limits there is a range of degrees of chaos. It is scaling in the sense that the classical dynamics is the same at all energies for a specific system (constant δ), apart from a time-scale. In terms of the previous two subsections, this means that all phase space structures remain the same at all energies, apart from their absolute sizes, all of which scale as $\sqrt{E}$. From a semiclassical perspective this allows for an increase in the number of states occupying a given region of phase space. However, at the same time areas are increasing, so are fluxes out of them (e.g. figure 13), which might allow for an increase in the quantum mechanical flow between regions.

By following the eigenstates of the oval billiard with parameter, their bifurcations can be studied in a continuous manner. Bifurcations as a function of energy are followed by moving along a progression, which requires skipping over eigenstates (figure 29). We also hope to separate the effects of avoided crossings from other changes which might occur in the eigenstates and smoothed states. It has been proposed that multiple avoided crossings lead to quantum chaos (Noid *et al.* 1980).

Figure 27 presents a series of shapes showing the way the oval billiard changes with δ. A correlation diagram for several states of a given symmetry is shown in figure 28. Because the billiards are similar to the particle in the box, it is convenient to express eigenvalues in terms of the wave-vector, k, with energy defined as follows:

$$E = k^2/2. \tag{9}$$

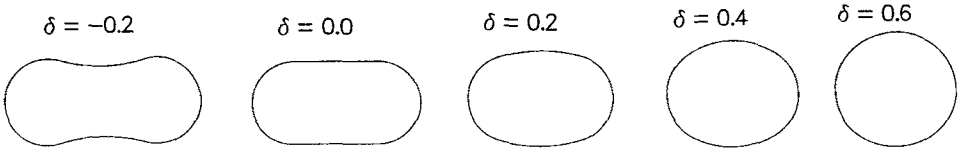

Figure 27. Plots showing how the shape of the oval billiard changes as a function of δ.

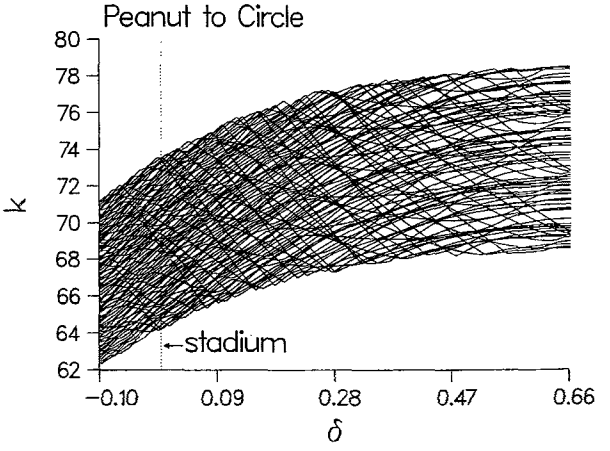

Figure 28. A correlation diagram for the eigenstates of the oval billiard which have even–even symmetry. The diagram includes adiabatic eigenstates 260–340.

Like systems (1) and (2), the stadium billiard eigenstates undergo bifurcations as energy is increased. The first 12 plots (up to 12 oe) of figure 29 demonstrate that there is a bifurcation from stretching to circulating eigenstates. Husimi transforms of the eigenstates are presented in figure 30, along with a separatrix, which is drawn with a thicker line. This separatrix is formed by following the stable and unstable manifolds of the periodic orbit (Lichtenberg and Lieberman 1992) which is at the centre of the plot (this orbit moves horizontally between the two semicircles on

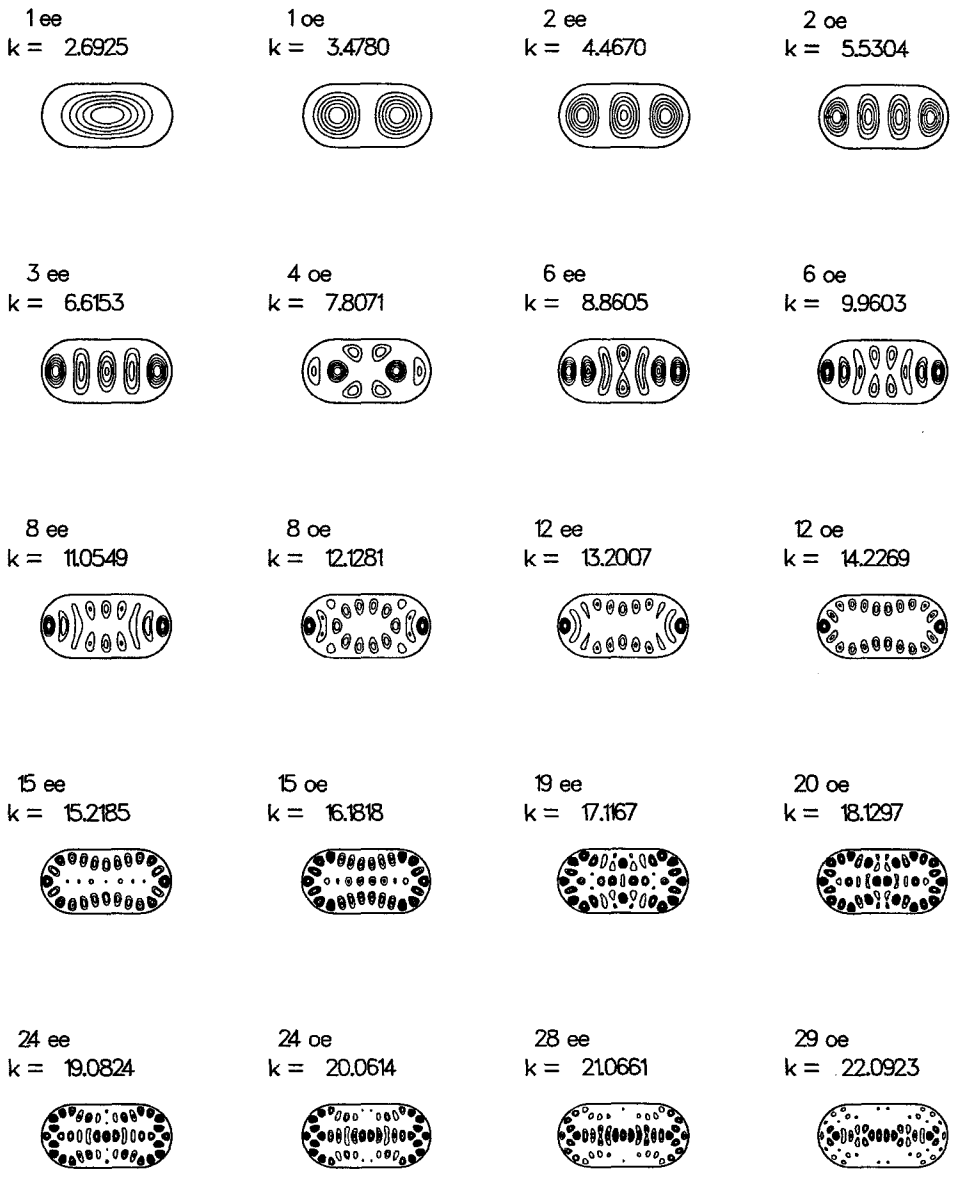

Figure 29. Low-lying eigenstates of the stadium billiard. The eigenstate 4 oe is in the middle of an avoided crossing.

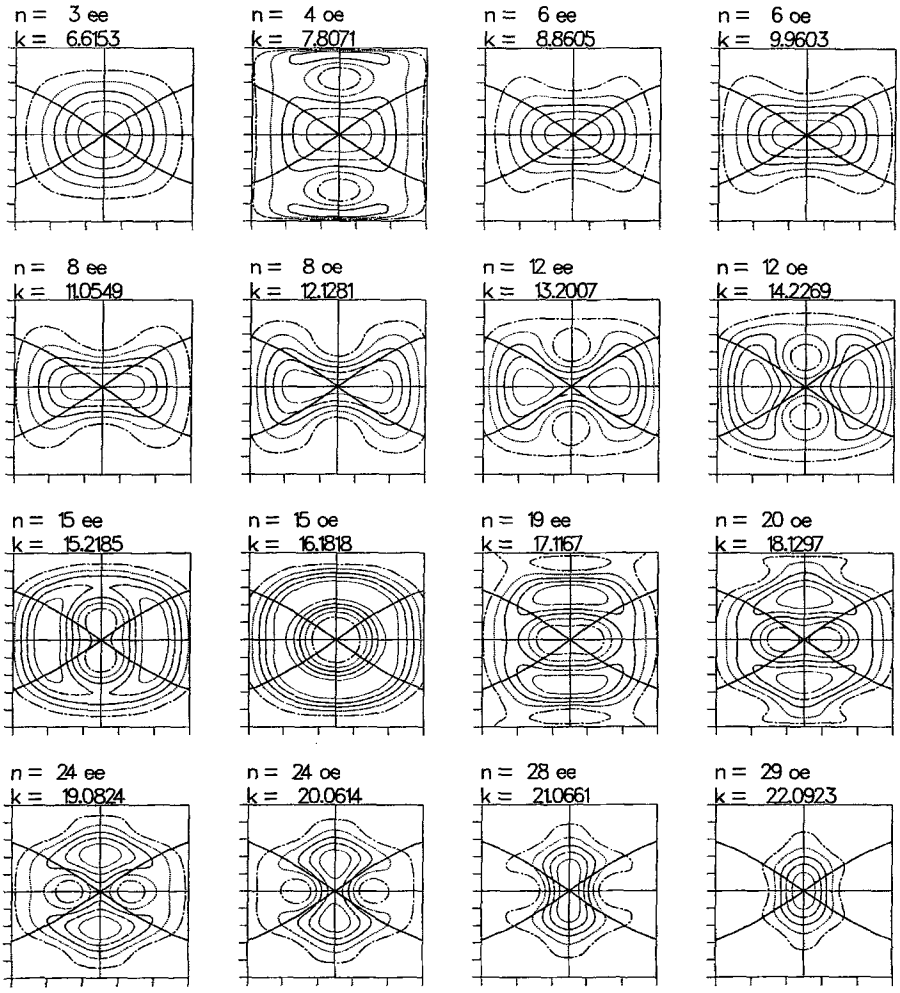

Figure 30. Husimi transforms of the eigenstates of figure 29. Included as a thick dark line is a broken-up separatrix. The line types have the same meaning as they do in figure 25.

either end of the stadium). It is the generalization to the stadium of the integrable separatrix which separates precessional from librational motion in the elliptical billiard (Keller and Rubinow 1960). The bifurcation is shown in phase space in the first eight plots of figure 30. First the maxima (dotted contours) lie right on top of the periodic orbit. As energy is increased the single maxima of each eigenstate split into two, which lie inside the separatrix (12 ee and 12 oe). Although these eigenstates have their maxima inside the separatrix, there is noticeable density outside it.

If this was the elliptical billiard, or an oval billiard with a higher value of δ, there would be a series of eigenstates after the first twelve of figure 29 for which the number of radial nodes would increase with energy, reflecting the fact the eigenstates, once inside the separatrix do not leave at all (elliptical billiard) or until much higher energy (non-integrable oval billiard with higher value of δ). Figure 31 shows an example of such a case for $\delta = 0{\cdot}3$.

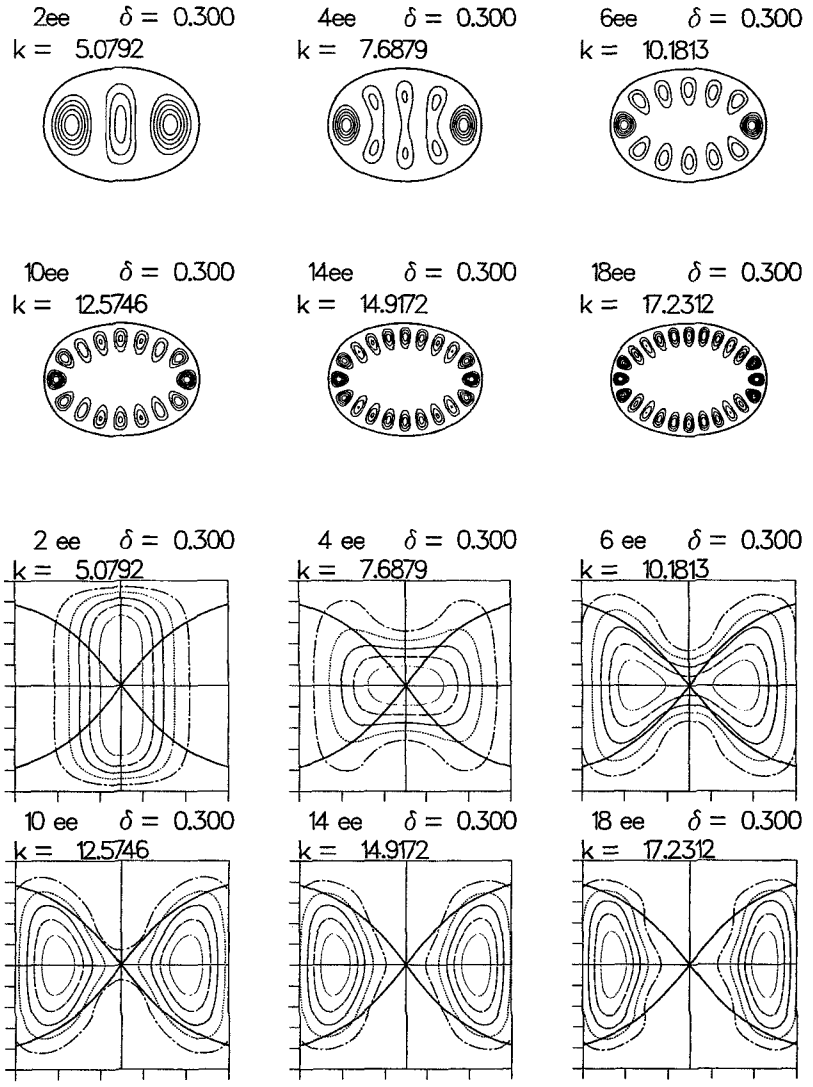

Figure 31. A bifurcation for the oval billiard with $\delta = 0{\cdot}3$. The top two rows show coordinate space plots and the bottom two Husimi transforms, which also include a separatrix.

The change in the eigenstates of the stadium evident in the last eight plots in figures 29 and 30 poses an interesting problem. Unlike the cases studied above, where the classical chaos is weaker, progressions of eigenstates do not remain inside the separatrix after they enter. The situation in figures 29 and 30 is interesting because it shows the breakdown of the picture presented in § 3.1. and several recent references (Gibson *et al.* 1987, Davis 1988, Radons and Prange 1988, Benito *et al.* 1989, Bohigas *et al.* 1993). The change also occurs for higher values of δ at higher energies, and we are pursuing an explanation presently. It is possible to make the qualitative argument that the eigenstates are headed in the direction of the classical

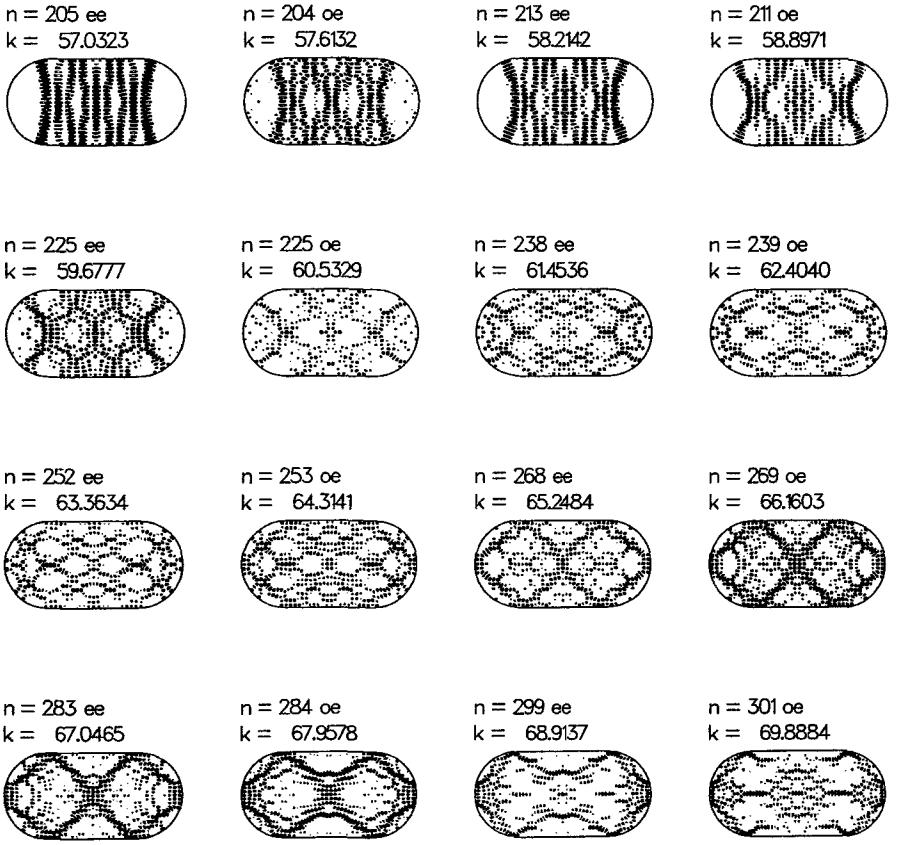

Figure 32. Plots which follow a localized eigenstate of the stadium (283 ee) to lower and higher energy.

flow, and since the flux across the separatrix is so large, this is bound to happen. But our goal is to develop a quantitative rationalization for this phenomenon, which seems possible because, while the eigenstates move outside the separatrix, they are still localized.

Bifurcations of eigenstates of the stadium also occur at higher energy, and figure 32 demonstrates this, showing plots which follow a single type of eigenstate. The type of eigenstate is shown in panels 11-14 (states 268 ee to 284 oe), and it has the shape of a double diamond. One of these eigenstates, 283 ee, has been presented previously by Heller (1984) as an example of a scar of a periodic orbit. These eigenstates demonstrate the difficulty in applying the approach of Heller either in its original form (Heller 1984) or a modified version (Heller 1991). Neither of his approaches can account for the trend pictured in the figure, the presence of a certain type of eigenstate for a narrow range of energy.

Figure 33 follows the double diamond state of the stadium as δ is varied. The eigenstate loses the double diamond shape in both directions in parameter space, a result that is once again difficult to rationalize with Heller's scar formalism. Bifurcations as a function of parameter will be discussed again in § 4.2., but at lower

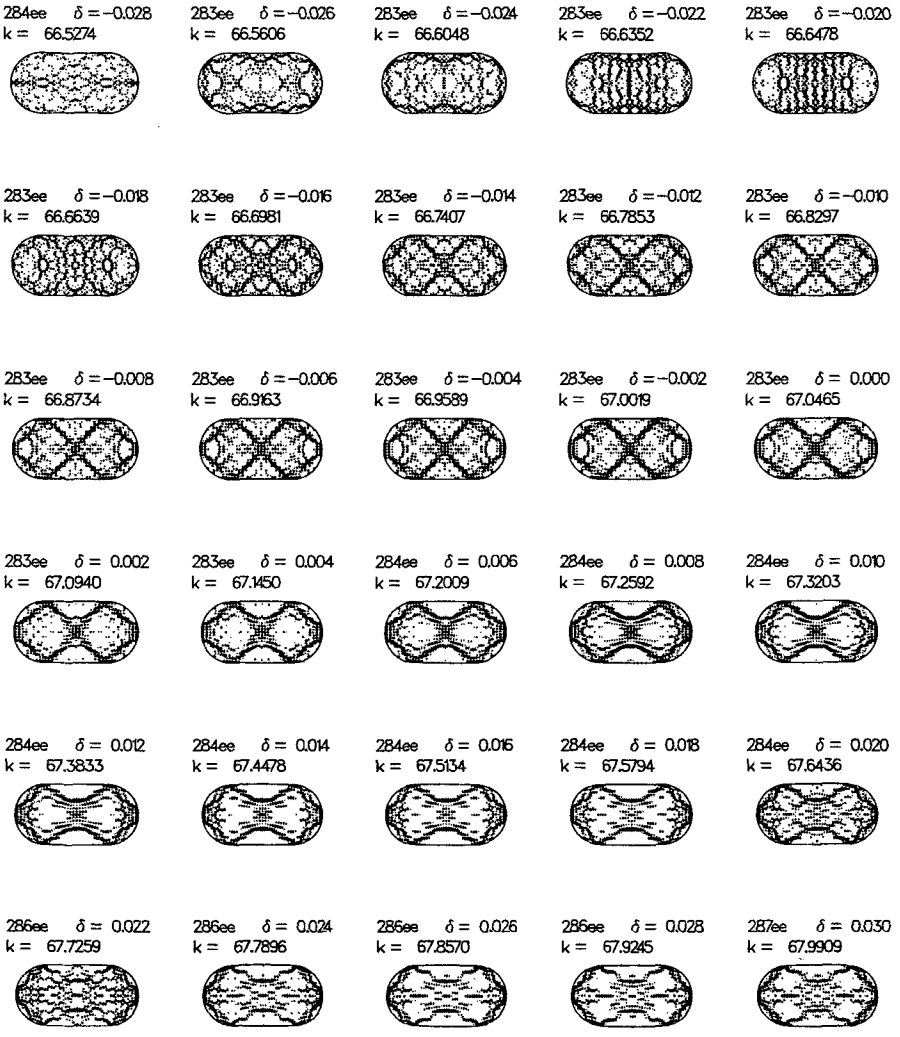

Figure 33. The 283ee state of the stadium (third row on the right) followed in parameter space.

energy and higher δ, where semiclassical analysis is more straightforward (there is less classical chaos and the flux across the separatrix is smaller).

4. Case studies

4.1. *Hierarchical analysis*

Figure 34 (*a*) shows a spectrum for a wavepacket moving in system (2) centred at (0·0, −34·77, $p_x(E)$, −0·256) with the same E, α_x, and α_y as the ones in § 3.2. Figures 34 (*b*)-(*f*) show a middle portion of smoothed spectra, and these can be compared to figure 14. The peaks in figure 34 (*c*) are more closely spaced than those in figure 14 (*c*), indicative of wavepacket motion which has slower recurrences.

The spectrum in figure 34 (*a*) has three distinct regions. The transitions between the regions may be difficult to observe in the stick spectrum, because of the size of

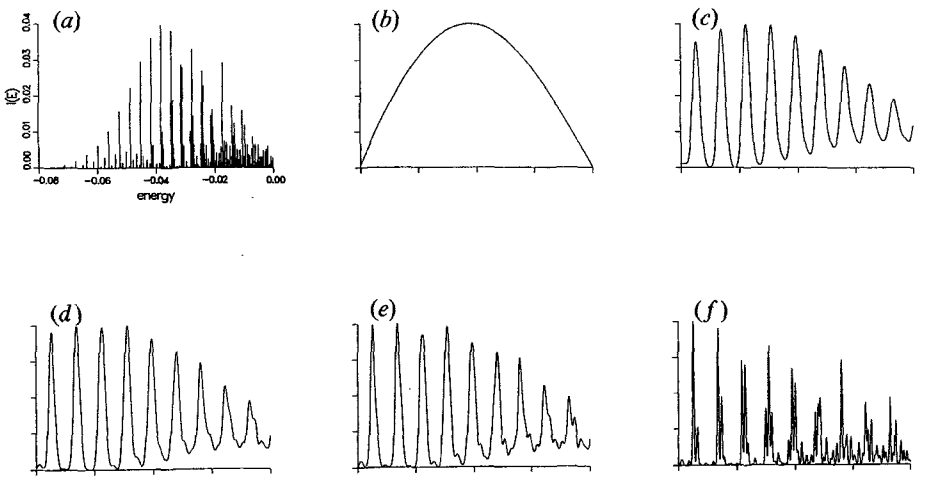

Figure 34. A spectrum (*a*) and smoothed spectra (*b–f*) for another wavepacket described in the text. The smoothed spectra are for a middle portion of the stick spectrum ($E = -0{\cdot}0402$ to $-0{\cdot}00754$).

the plot. The first transition is evident on figure 34 (*d*) and (*e*), where there is a shift in location of the side peak from the left to the right side as energy is increased, but is more obvious in the hierarchical tree representation in figure 35. A series of nodes between 0·1 and 0·2 starting at the left become lower in the middle of the plot. The second transition occurs at high energy, evident in the higher nodes on the far right side of the tree. To better view the branching of the tree in figure 35, a series of subtrees are presented in figure 36, which were cut from the tree above 0·2. These subtrees correspond to the peaks of figure 34 (*c*).

A set of smoothed states are plotted in figure 37 which are at the same resolution as figure 34 (*c*). Although the shapes of the states are distorting with increasing excitation, they form an overtone progression in a coordinate system which is evolving with energy. The number of nodes starts at two in the first plot on the

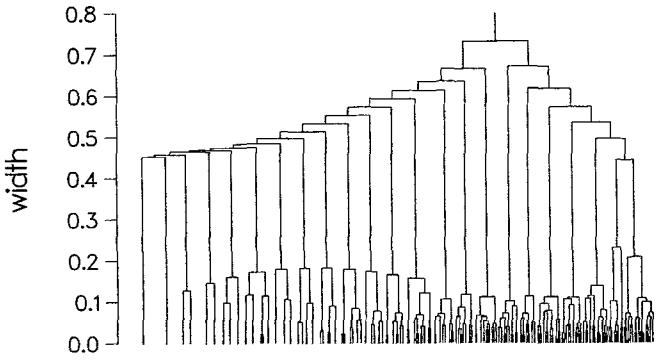

Figure 35. A tree from the spectrum of figure 34 (*a*). The widths are scaled in the same way as figure 15.

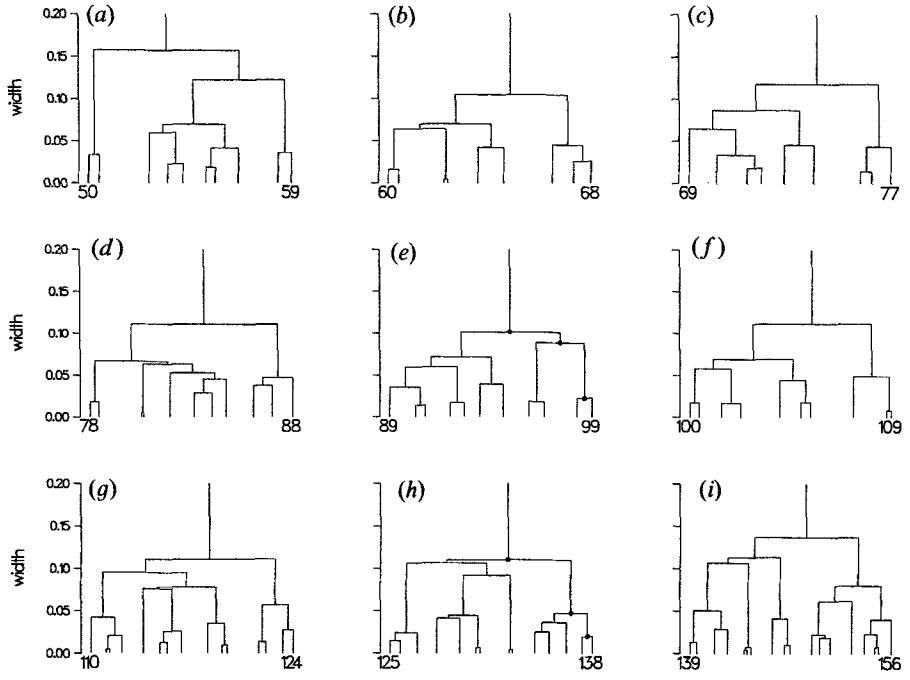

Figure 36. Subtrees generated by cutting the tree of figure 35 just above a width of 0·2.

upper left and ends at 21 in the last plot on the lower right. Comparison of figures 3 and 37 once again emphasizes the utility of the smoothing. There is no strong evidence in figure 3 for the type of localization observed in figure 37. The states in figure 37 can be compared with the eigenstates in figure 1, which are their parents.

The transitions in the spectrum of figure 34 (*a*) are evident in smoothed states at a higher level of resolution. Figure 38 shows 15 pairs of states which result from cutting subtrees like those in figure 36 above their second highest nodes. The first transition occurs in the middle row where the order of the pairs switches (the overtones are associated with the larger peaks in figure 34 (*d*)). In the middle pair of the middle row one of the smoothed states (66–68) becomes a bit jumbled, but then a pattern emerges. The states 86–88, 96–99 and 107–109 are distorted by a 3:2 classical resonance. Later the second transition occurs and the last two states associated with the smaller peaks change appearance (bottom right). These states are effected by the 2:1 resonance zone described above.

The smoothed states in figure 38 are another example of the divide and conquer aspect of the hierarchical analysis. These states were chosen from the hierarchical analysis by cutting subtrees above their second highest node, not by cutting the full tree at a given height, and thus these states are not all at the same level of resolution, or time-scale. The need for this can be observed in figure 34. In figure 34 (*d*) some of the side peaks are not developed, and in figure 34 (*e*) when all side peaks are developed, there are additional peaks.

The results presented in this subsection and the analysis of the phase space structure of system (2) (Davis 1994b), suggest the following reason for the first transition. At low energy there is either no 3:2 resonance or there is not enough

phase space in the 3:2 resonance, and the smoothed states do not reflect resonant motion. At higher energy there is enough phase space to support states and the smoothed states are influenced by the resonance. The onset of the classical resonance is the reason for the breakdown of the progression in figure 1. The classical chaos becomes severe in this system and '3:2 resonance' is used in the sense of § 3.1. That is, there is a resonance zone which has a flux out of it smaller than the quantizable action, or the dynamics is localized inside the resonance zone for a time sufficient for it to be reflected in the smoothed states.

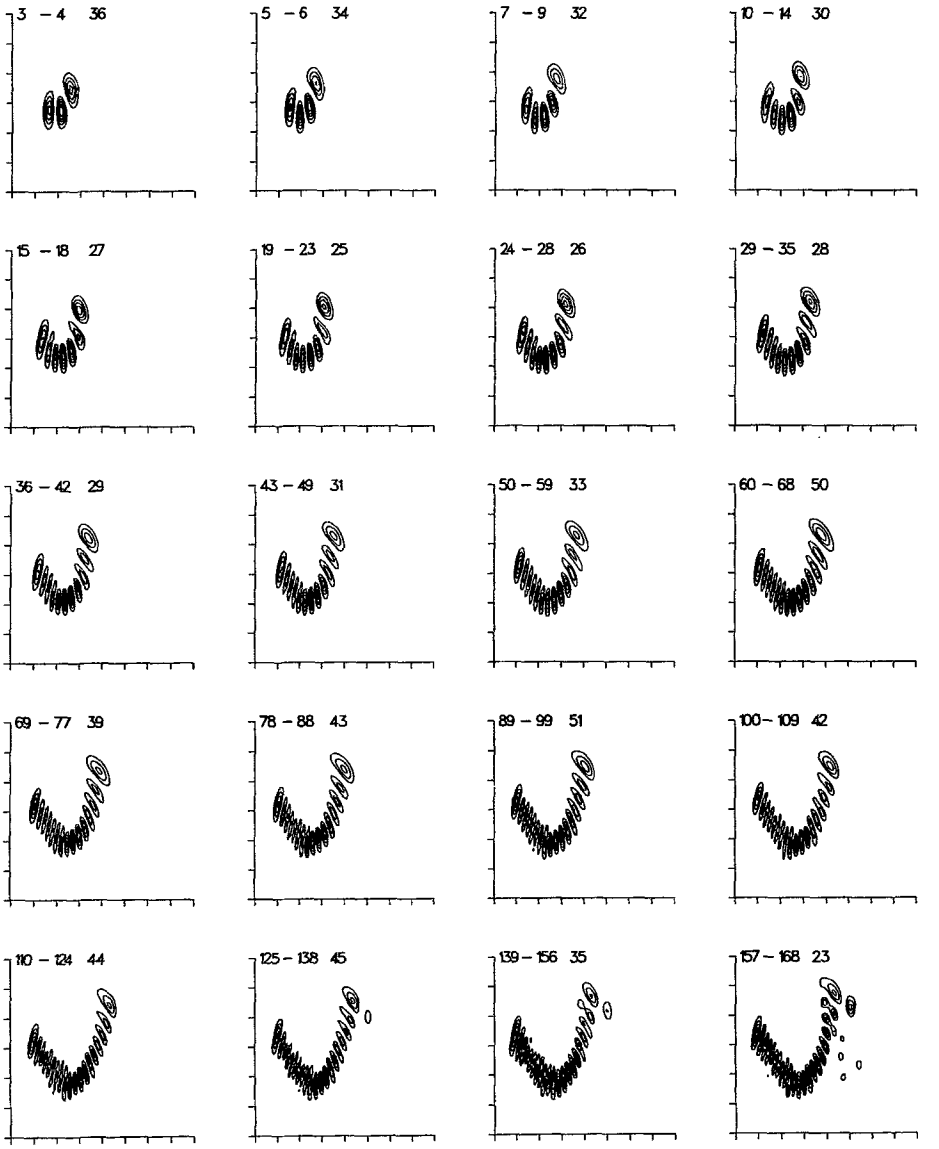

Figure 37. Smoothed states generated from groups resolved by cutting just above 0·2 in figure 35. Some of the subtrees for these states are shown in figure 36.

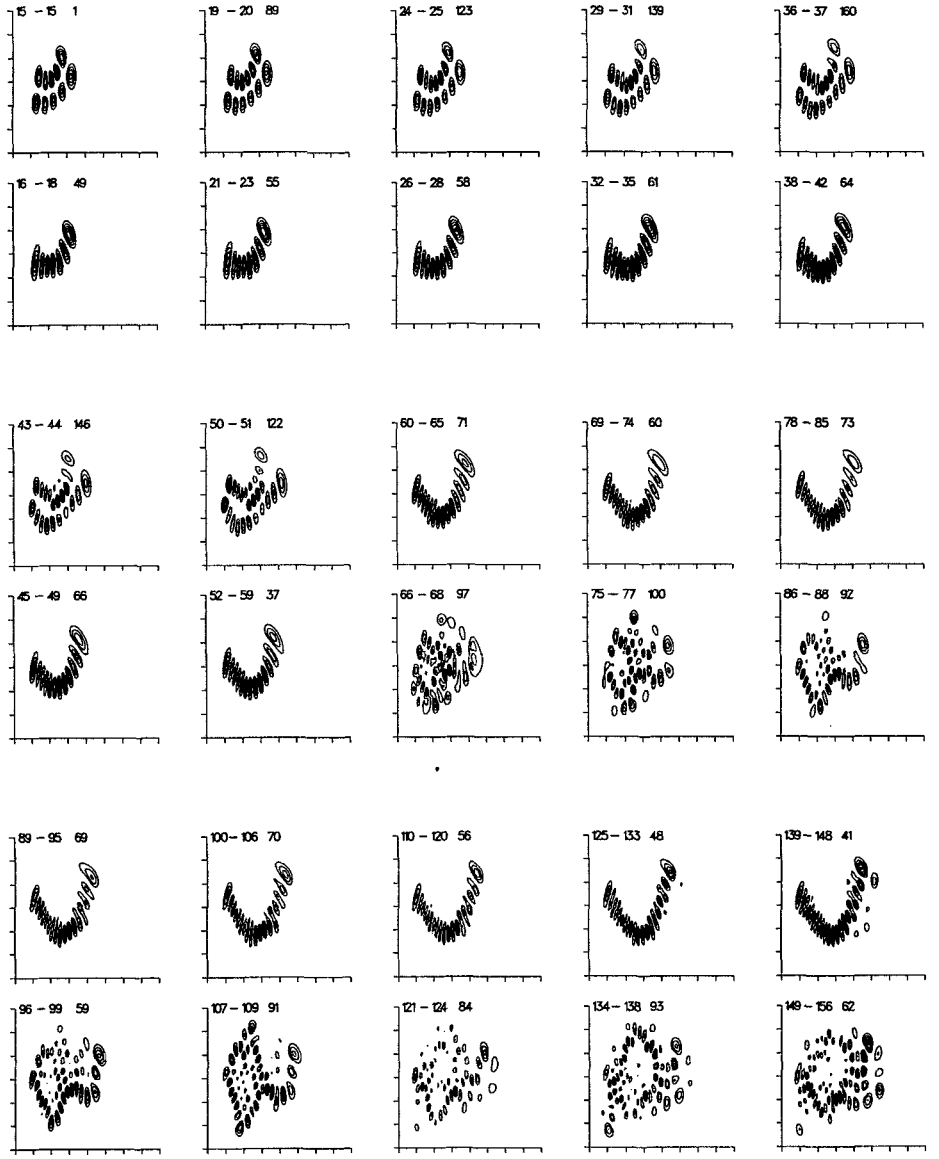

Figure 38. Pairs of states corresponding to the larger and smaller peaks of figure 34 (*d*) and (*e*). The states which look like those in figure 37 are for the higher peaks.

The second transition results from the breakdown of the effect of the 3:2 resonance zone. There are four plausible reasons why this happens. First, the resonance zone may become too small to support quantum states. Second, the resonance may disappear entirely at higher energy. A third possibility is that the flux out of the resonance may become too large for it to support states. A fourth possibility is that the phase space structure distorts sufficiently that a wavepacket which is centred inside the resonance zone at low energy, no longer is prominently inside at high energy. Figures 39 and 40 suggest that the reason is one of the first

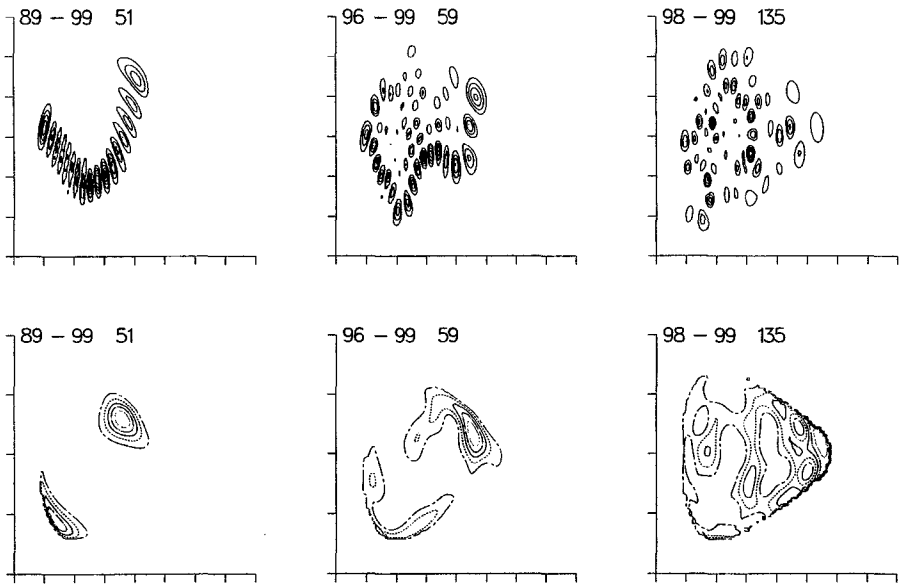

Figure 39. A decay pathway for one of the states of figure 37 (fourth row). The path for this state is on figure 36(*e*). The top row shows coordinate space plots and the bottom Husimi transforms of the same states.

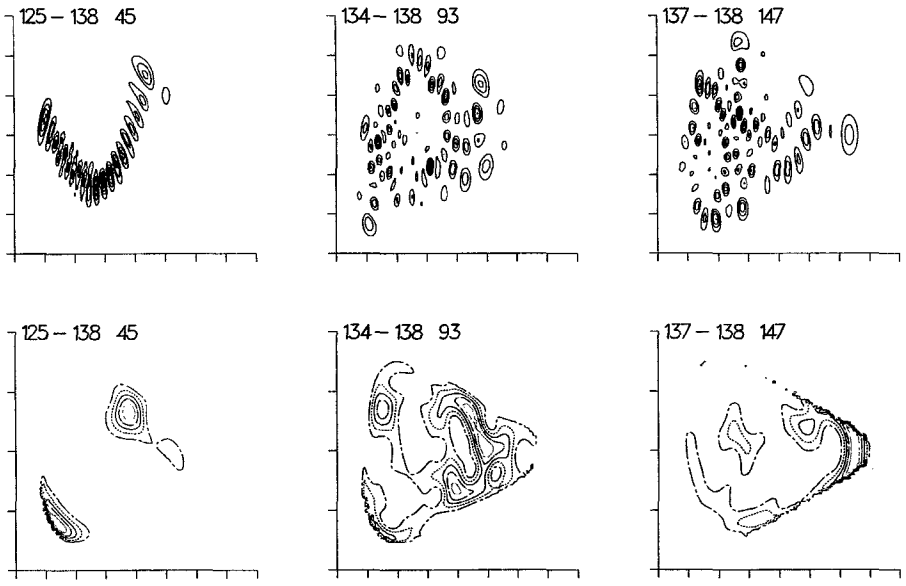

Figure 40. A decay pathway for another state of figure 37 (bottom row). The path for this state is on figure 36(*h*).

three. Figure 39 shows results for one of the overtone states from figure 37 and figure 40 shows results for another. These are pictured in the upper left of each figure in coordinate space and a Husimi transform is presented on the lower left of each figure. Each then shows the results of paths down their respective subtrees, which are illustrated with dots in figure 36(*e*) and (*h*). The overtone state of figure 39 first shows the effects of a 3:2 resonance, and then spreads into another region of phase space.

The remainder of figure 40 shows the development of the higher energy overtone state. Note again that this state misses the 3:2 resonance zone, which is also evident in the Husimis. The last picture in the sequence shows that a piece of the overtone state has entered into a different region of phase space, which was present on the left column of figure 25, a 5:3 resonance zone. Comparison of the last column of figure 39 with the middle column of figure 40 indicates that a piece of the lower energy overtone state enters a region of phase space similar to the initial excursion of the higher energy overtone. The comparison of figures 39 and 40 lends credence to the first three of the four possible reasons for the second transition. The higher energy overtone is in a position to be influenced by the 3:2 resonance zone, but is not.

4.2. *Oval billiard*

4.2.1. *Hierarchical analysis*

Figure 41 shows portions of a stick spectrum in the left two panels and smoothed versions of the second panel in the right two panels. The spectrum was generated with a wavepacket like the one in equation (4), but it is adjusted to have the same boundary conditions as the stadium and (α_x, α_y) are set by the classical energy of the centre of the wavepacket (Davis 1994c). Although the stick spectrum

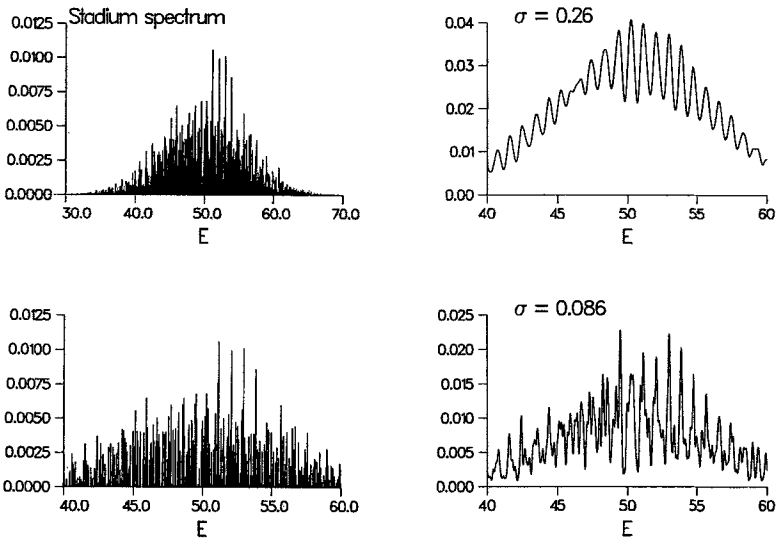

Figure 41. A spectrum for a wavepacket in the stadium in the top left plot, a middle portion of the same spectrum in the bottom left plot, and smoothed versions of this middle portion in the right two plots.

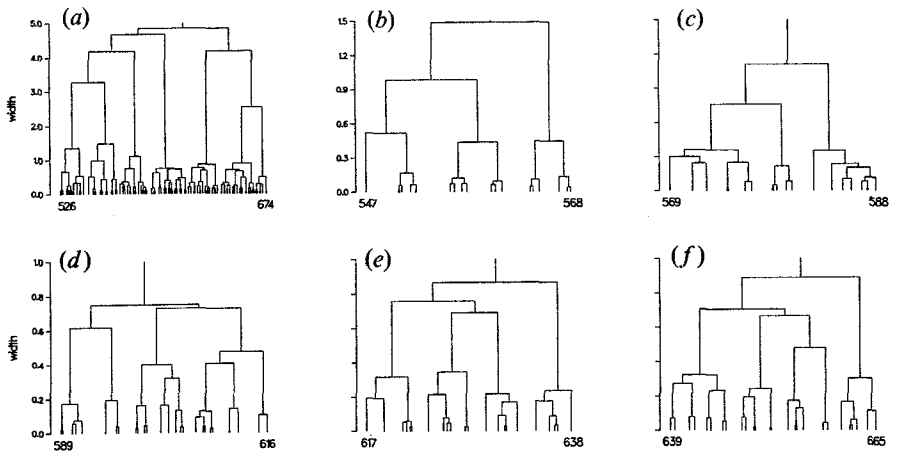

Figure 42. A tree (*a*) from the spectrum of figure 41, followed by a set of subtrees. Width refers to a scaled version of σ. To convert width to σ, multiply by 0·142.

appears complicated, the smoothed spectrum in the third panel shows regularity superimposed on a broad background. The level of smoothing in the third panel was chosen from the hierarchical representation of the spectrum which is shown in figure 42(*a*) along with subtrees in figures 42(*b*)-(*f*). The subtrees correspond to five of the peaks in the smoothed spectrum in the third panel of figure 41 ($E = 48{\cdot}0\text{-}52{\cdot}0$).

The subtrees show many strong groupings, based on the differences in nodal heights. For example, the subtrees in figure 42(*b*) and (*c*) show strong propensities for three groups, the one in figure 42(*d*) shows a weaker propensity for three groups, the one in figure 42(*e*) shows a strong propensity for four groups, and the subtree in figure 42(*f*) shows a propensity for either four or five groups. The groupings in figure 42 are comparable to those in figure 36, based on a statistical analysis (Davis 1993). So it seems likely that much of the analysis of energy transfer pathways presented in §§ 3.2. and 4.1. and Davis (1994a, b) could be used to understand the quantum dynamics and the classical-quantum correspondence for the stadium.

Figure 43 presents smoothed states for the subtrees of figure 42. Like some of the previous results (figure 23), the smoothed states appear to be part of a progression, but are difficult to assign. These states are noticeably different than their parents in figure 44, indicating extensive energy transfer, which is not surprising considering the chaotic classical dynamics of the stadium.

4.2.2. *Diabatic states*

As noted in § 3.3., a good way to study bifurcations of eigenstates is to follow them in parameter space. To do this the eigenstates must be followed through avoided crossings, and we refer to these as 'diabatic states'. They are not diabatic in the usual sense, because the eigenstates are followed by jumping onto a new adiabatic curve at an avoidance. The jump is done based on an investigation of the correlation diagram and coordinate and phase space plots of the eigenstates. This is not a foolproof way to follow the eigenstates, but all the methods we could think of encounter difficulties at broad avoidances.

Figure 45 shows a portion of the correlation diagram for the oval billiard (even-even eigenstates). Superimposed on it is a line of large dots which is an estimate of a diabatic state in the sense described above. Although this state is straightforward to follow through most of the avoidances, difficulties arise at the large avoidance near 0·14, and at high δ, where there are several close adiabatic curves. Figure 46 shows a series of eigenstates along the diabatic curve. A bifurcation occurs between $\delta = 0{\cdot}2$ and 0·5 like the one pictured in figures 29–31. The first four plots in figure 46 ($\delta = -0{\cdot}1$ to 0·2) are also interesting because the first three eigenstates are similar and there is a significant change at the fourth, after the broad avoidance noted above.

Figure 47 shows a set of diabatic curves as defined above. The curve in the lower right is the one drawn on figure 45. In these plots it is often difficult to extrapolate from before an avoidance to after one. This sort of discontinuity is different from the usual view of what occurs at an avoidance, for example in the problem of two potential energy curves (for example, chap. XI of Landau and Lifshitz 1977). In that case, the potential curves are derived from a Hamiltonian where some of the terms are left out and there are well defined off-diagonal matrix elements which couple the curves. The curves in figure 47 are the actual eigenvalues, and it may be difficult to define off-diagonal matrix elements for them.

4.2.3. *Semiclassical analysis of the bifurcation of the eigenstates*

Figure 48 shows a series of separatrices like those presented earlier (figures 30 and 31). The separatrix gets larger as δ increases and figure 49 shows how the last six eigenstates of figure 46 behave relative to it. The eigenstate at $\delta = 0{\cdot}2$ has a peak which lies outside the separatrix and the eigenstates at $\delta = 0{\cdot}5$, 0·6 and 0·66 have densities which lie largely inside the separatrix, an indication of the bifurcation. The eigenstates at $\delta = 0{\cdot}3$ and 0·4 appear to lie right on the separatrix. Owing to its elongated shape, it is assumed that semiclassical quantization conditions exist outside the separatrix for the eigenstate at $\delta = 0{\cdot}3$. Tunnelling across the separatrix causes the state to develop a maximum right at the periodic orbit (Davis 1988).

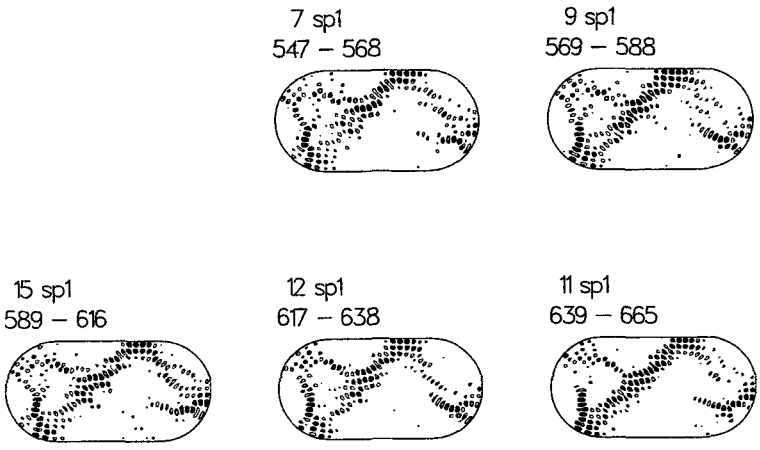

Figure 43. Smoothed states for the subtrees of figure 42 (*b–f*) are shown. The real parts of the states are plotted.

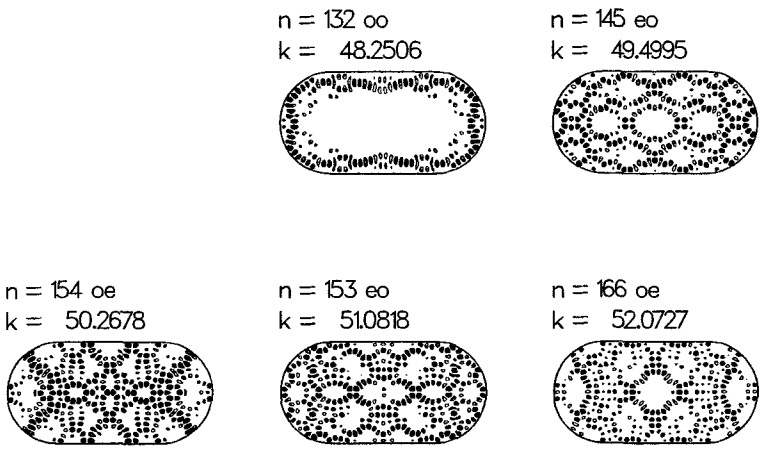

Figure 44. Parent eigenstates of the smoothed states of figure 43.

The analysis can be made more quantitative by measuring the area inside the separatrix as a function of δ, as shown in figure 50 (*a*). The area is calculated at $k=1$ (equation 9). Since the billiards are scaling systems, the area at any value of k can be calculated via the following relationship:

$$A_k = k\, A_1, \tag{10}$$

where A_1 is the area inside one half of the separatrix at $k=1{\cdot}0$ and A_k is the area at some other value of k. To make an estimate of where the bifurcation takes place the one-dimensional quantization condition

$$A_q = (n+1)\, h \tag{11}$$

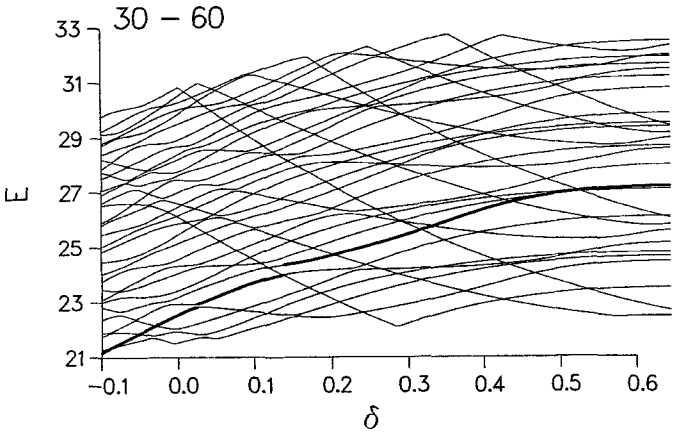

Figure 45. A diabatic curve (thick dots) is plotted here along with several adiabatic curves (30–60).

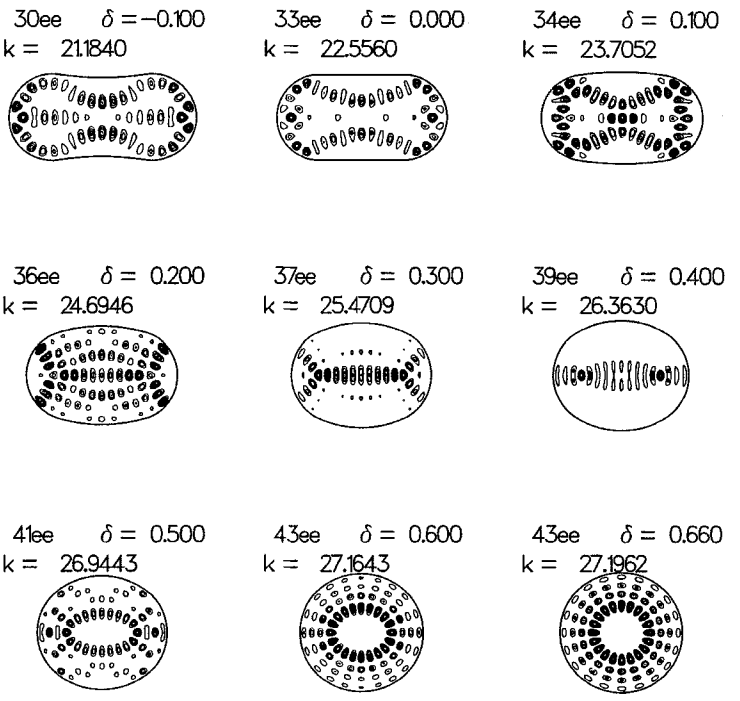

Figure 46. Eigenstates which lie along the diabatic curve of figure 45.

is used, where A_q refers to the quantizable area. Since $\hbar = 1{\cdot}0$, and area at $k = 1{\cdot}0$ has been calculated, we write the following relationship:

$$k_q = \frac{2(n+1)\,\pi}{A_1}. \tag{12}$$

Figure 50 (*b*) shows this curve for $n = 3$, the value for the diabatic state studied here, and also includes the diabatic curve. These curves cross between $\delta = 0{\cdot}412$ and $0{\cdot}414$. The accuracy of this estimate is assessed in figure 51, where Husimi transforms of the eigenstates near these values of δ are presented. Based on the shape of the Husimi transforms, it is estimated that the eigenstate crosses the separatrix at $\delta = 0{\cdot}36$, where the separatrix cuts across a set of ridges. The estimate is approximate, because there is only one quantum condition and the Husimi transform is a smooth version of the Wigner transform (Heller 1976), which is a more natural choice for studying such things. This estimate is reasonable, considering the degree of chaos near the separatrix (Davis *et al.* 1991).

4.2. *Photodetachment spectrum of $OHCl^-$*

Photodetachment spectra have proven to be an interesting way to probe the dynamics of ground state potential energy surfaces near or at the transition state, and the study of such spectra has been referred to as 'transition state spectroscopy'. We refer readers to two recent reviews (Schatz 1990, Metz *et al.* 1992), and recent papers (Bradforth *et al.* 1993, Grayce *et al.* 1993, Davis *et al.* 1994).

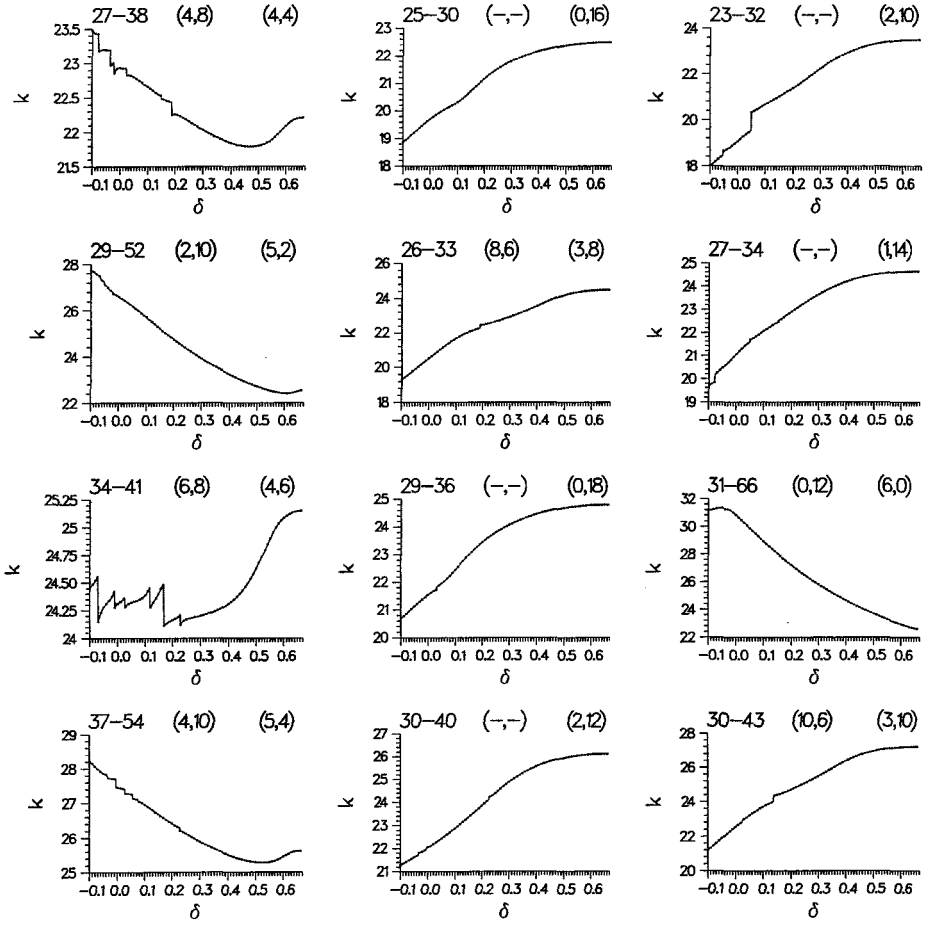

Figure 47. A series of diabatic curves. The curve from figure 45 is on the bottom right. The headings include the range of adiabatic curves (for example 27–38 on the upper left). Each plot also includes two pairs of numbers. The first set are the Cartesian quantum numbers (n_x, n_y) which can be assigned previous to bifurcations like the one in figure 46. In several cases Cartesian quantum numbers could not be assigned and (-,-) is indicated. The second pair of numbers show the radial and angular nodes, with the first number being radial. The designations of (10, 6) and (3, 10) (bottom right) can be compared with the pictures in figure 46.

Theoretical results for OHCl were generated from an L^2 basis set calculation (Davis *et al.* 1994) in the manner of Bowman and co-workers (Gazdy and Bowman 1989). This makes the scattering problem similar to the bound problem for which the hierarchical analysis was developed, and thus can be used in this case. Although the L^2 nature of the calculation is approximate, the hierarchical analysis can be used to discern at what level of resolution the calculation is accurate through examination of the smoothed states (Davis *et al.* 1994).

Figure 52 shows the tree generated from the theoretical version of the $OHCl^-$ photodetachment spectrum. It is presented in two pieces corresponding to the two peaks of figure 53. The bottom row of figure 53 shows smoothed states associated

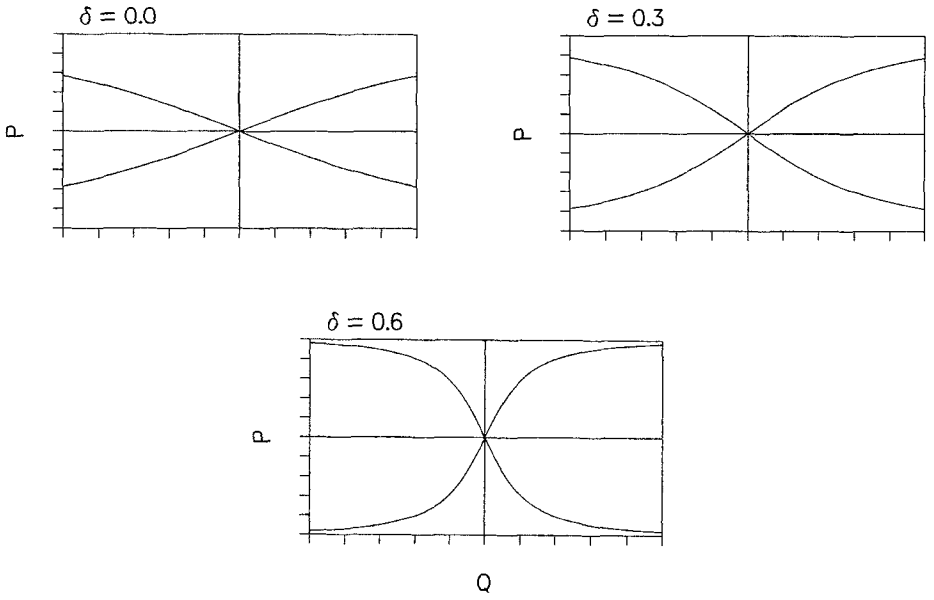

Figure 48. The broken-up separatrix for the oval billiard as a function of δ. These are (y, p_y) surfaces of section.

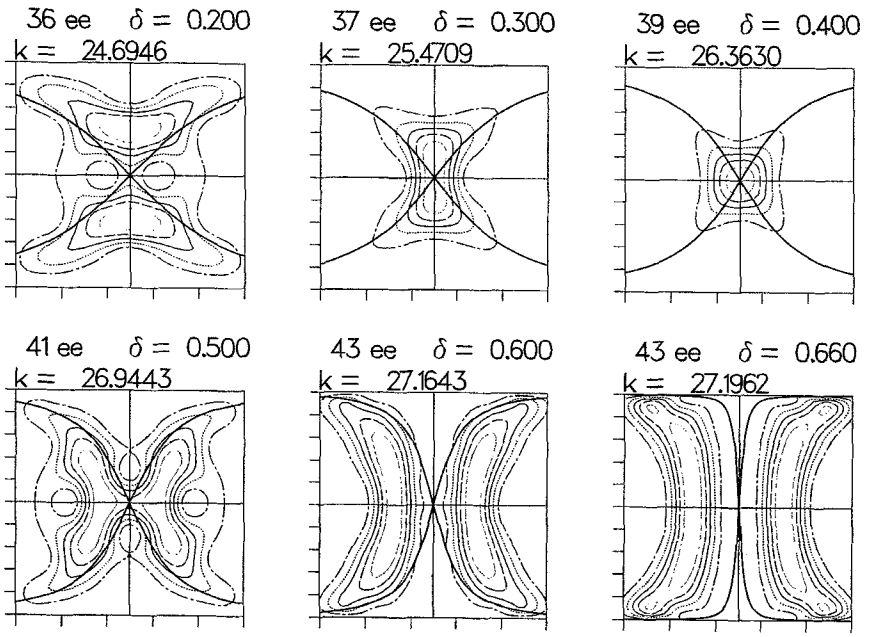

Figure 49. Husimi transforms of some of the eigenstates of figure 46 plotted along with the relevant separatrix to demonstrate how the bifurcation occurs in phase space.

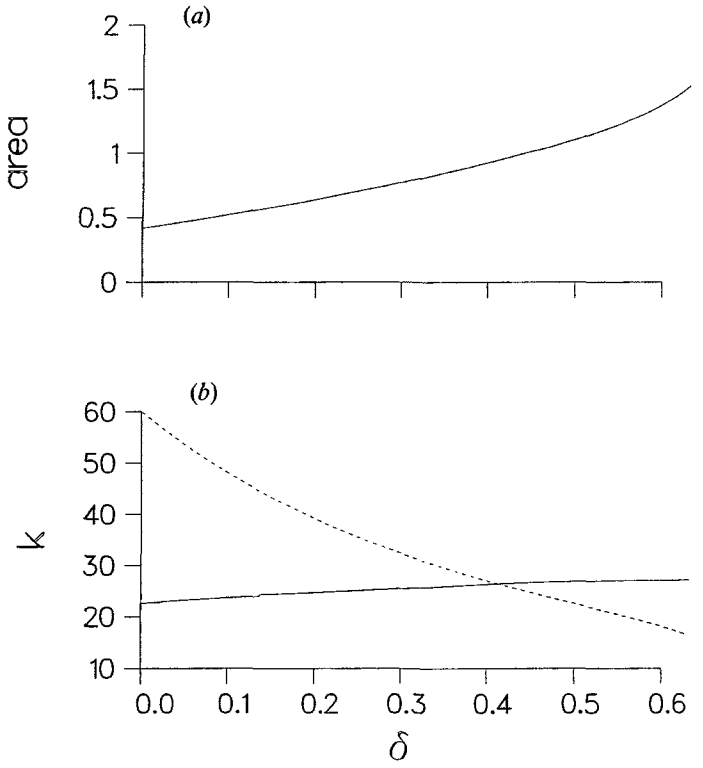

Figure 50. The top plot shows the area inside the separatrix as a function of δ. The bottom plot shows the diabatic curve from figure 45 as a solid line, along with the one-dimensional quantization condition of equation (12).

with the peaks above them plotted on top of potential contours (dotted lines) for the OHCl potential surface. The coordinate system in these plots is Jacobi, with the centre of mass of OH at (0, 0) and the Cl-atom fixed along the x-axis at $R=5{\cdot}9107$ au (R is the distance from the Cl atom to the centre of mass of OH). The H-atom is allowed to move in the plane of the O–Cl bond. Figure 53 demonstrates that the states are a short progression in an H-stretch which is mostly OH in character, thus assigning the two peaks.

Figure 54 presents a higher resolution version of the first peak in figure 53. The level of resolution was chosen from the tree on the top of figure 52, where there is a large gap between the eighth and ninth nodes. The smoothed spectrum has regularly spaced peaks which fit an OH rotor spectrum and the bottom four plots in figure 54 investigate this. These plots have the same axes limits as those in figure 53 and are generated at the same value of R. These smoothed states confirm the OH rotor assignment of the peaks above them, but they are truly above barrier hindered rotors, because they become pinched as they cross $y=0{\cdot}0$ near $x=2{\cdot}0$ (collinear).

5. Conclusions

In this paper I have reviewed work on the analysis of highly excited vibrational eigenstates. The analysis seems useful, because of the success researchers have had in

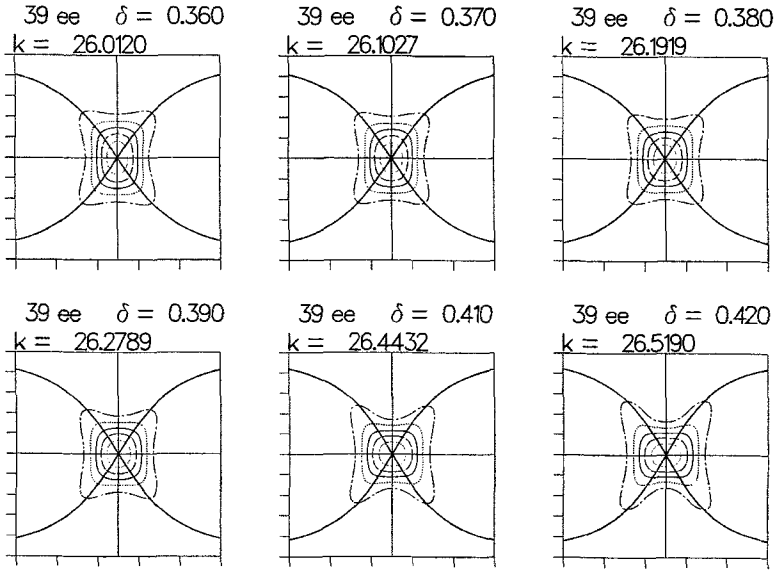

Figure 51. More Husimi transforms along the diabatic curve of figure 45 are plotted along with a separatrix.

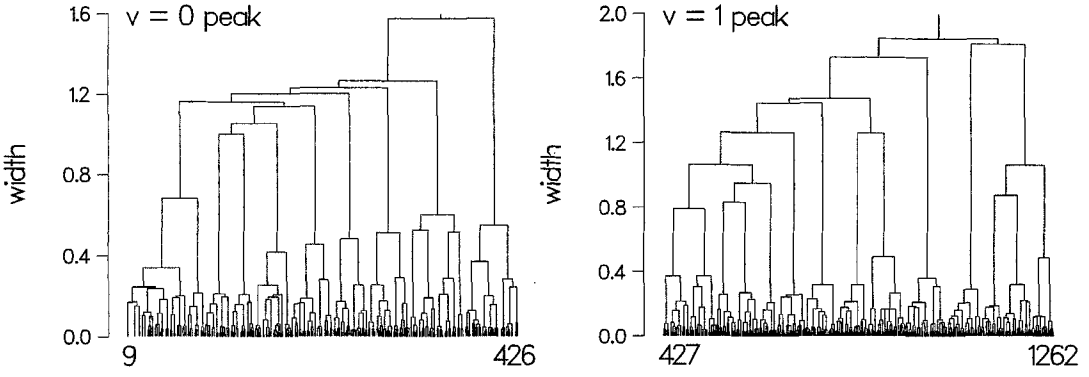

Figure 52. Two subtrees for the $OHCl^-$ photodetachment spectrum. The numbers at the bottom list the lines from the L^2 calculation. The widths have been scaled and can be converted to σ by multiplying by 0·01501.

finding the eigenvalues of triatomic and tetra-atomic molecules (see the reviews by Bacic and Light (1989), Sibert (1990), the collection of articles in Bowman and Ratner (1991), and recent articles on the vibrational eigenstates of acetylene by Bentley *et al.* (1992), Sibert and Mayrhofer (1993), for example). With the possibility of generating hundreds or perhaps thousands of eigenstates, it seems that there will be a need for processing this information, because a cursory examination of either eigenstates or wavepacket dynamics may be difficult to interpret. This point was

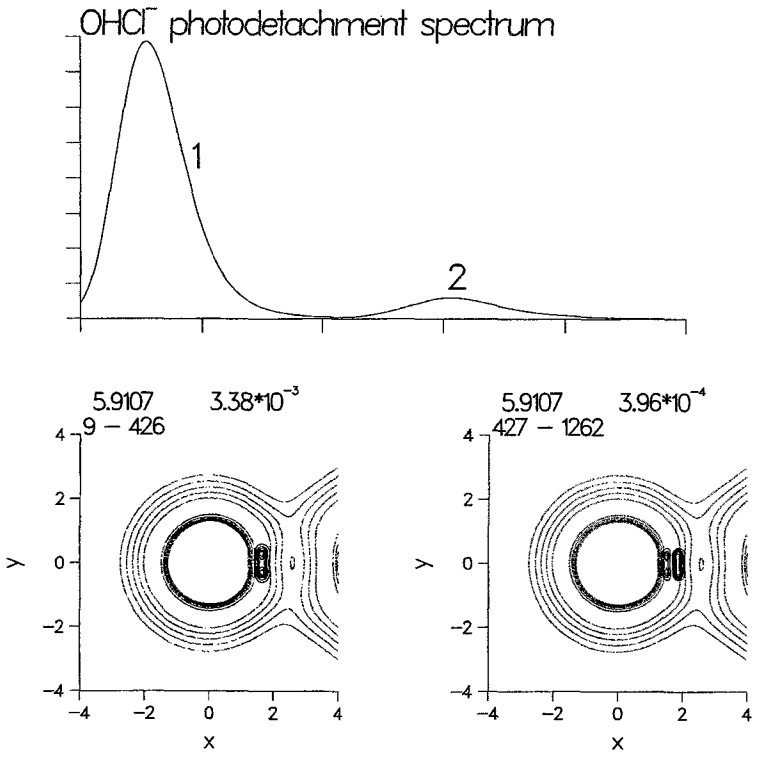

Figure 53. A smoothed version of the photodetachment spectrum is shown on the top and the bottom plots show smoothed states associated with the two peaks. Also included with the smoothed states are potential contours. These states are plotted in a coordinate system described in the text, with $R = 5{\cdot}9107$ au, as indicated on each plot. The headings also include the maxima of the states and the range of lines used from the L^2 calculation.

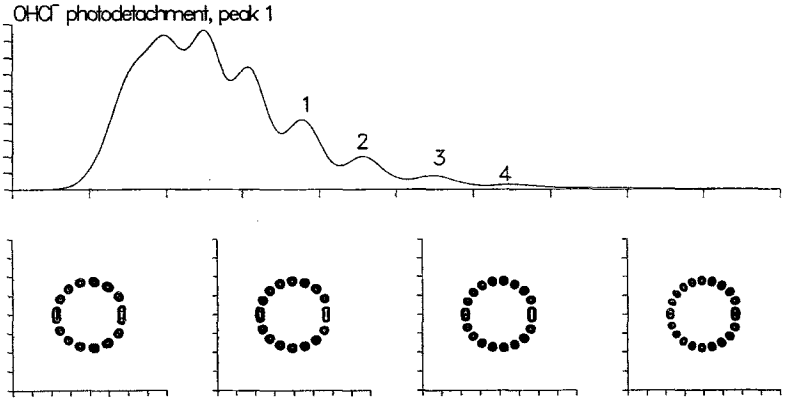

Figure 54. A higher resolution version of the first peak of figure 53 is shown on the top. The bottom plots are smoothed states associated with peaks 1–4. These are hindered rotor states with the value of J running from 7 to 10.

discussed in some detail in §2.3., with figures 3–5 and 7 pointing to such a need. Another, related reason for the analysis is the complexity of spectra of highly excited molecules. Given a model of a spectrum based on the eigenstates, it is possible to assign it and to understand the intramolecular dynamics associated with the spectrum in a relatively straightforward manner using the hierarchical analysis. I also wish to point to the utility of the semiclassical and hierarchical analyses for the question of the classical–quantum correspondence in systems which are classically chaotic, as discussed in §§3.3. and 4.2.

Future work is proceeding in several directions. First of all, more applications are planned, with the study of the intramolecular dynamics of HO_2 (Gazdy and Bowman 1992) at a preliminary stage. We also plan to make a more explicit connection between the semiclassical and hierarchical analyses, rather than the implicit connection made so far (i.e. interpretation of the hierarchical analysis was based in part on the phase space structure). Finally, I wish to emphasize a continuing interest in the issue of the quantum mechanical manifestations of classical chaos discussed in §4.2. It seems particularly worthwhile to study such issues along a correlation diagram for two reasons. First, the bifurcations of eigenstates can be studied in a continuous manner, and second, the role of avoided crossings can be assessed. Finally, I wish to note again the interesting phenomenon presented in §4.3.: the apparent discontinuity in the 'diabatic' states on either side of an avoided crossing (put more precisely, the apparent lack of simple extrapolation).

Acknowledgments

I would like to thank Professors Craig Martens and Robert Littlejohn for the use of computer codes employed in the study of the oval billiard, as well as helpful discussions. This work was supported by the Office of Basic Energy Sciences, Division of Chemical Sciences, US Department of Energy, under Contract No. W-31-109-ENG-38.

References

BAI, Y. Y., HOSE, G., STEFANSKI, K., and TAYLOR, H. S., *Phys. Rev.* A, 1985, **31**, 821.

BACIC, Z., and LIGHT, J. C., 1989, *Ann. Rev. phys. Chem.*, **40**, 469.

BENITO, R. M., BORONDO, F., KIM, J. H., SUMPTER, B. G., and EZRA, G. S., 1989, *Chem. Phys. Lett.*, **161**, 60.

BENNETTIN, G., and STRELCYN, J.-M., 1978, *Phys. Rev.* A, **17**, 773.

BENTLEY, J. A., WYATT, R. E., MENOU, M., and LEFORESTIER, C., 1992, *J. chem. Phys.*, **97**, 4255.

BOHIGAS, O., TOMSOVIC, S., and ULLMO, D., 1993, *Phys. Rep.*, **223**, 43.

BOWMAN, J. M., and RATNER, M. A., 1991, *Advances in Molecular Vibrations and Collision Dynamics*, **1***A* and **1***B* (Greenwich: JAI).

BRADFORTH, S. E., ARNOLD, D. W., NEUMARK, D. M., and MANOLOPOULOS, D. E., 1993, *J. chem. Phys.*, **99**, 6345.

BRODY, T. A., FLORES, J., FRENCH, J. B., MELLO, P. A., PANDEY, A., and WONG, S. S. M., 1981, *Rev. mod. Phys.*, **53**, 385.

BROWN, R. C., and WYATT, R. E., 1986a, *Phys. Rev. Lett.*, **57**, 1; 1986b, *J. phys. Chem.*, **90**, 590.

BUNIMOVICH, L. A., 1974, *Funct. Anal. Appl.*, **19**, 254.

BUNKER, D. L., and HASE, W. L., 1973, *J. chem. Phys.*, **59**, 4621.

BURLEIGH, D. C., and SIBERT, E. L., 1993, *J. chem. Phys.*, **98**, 8419.

CALIFANO, S., 1976, *Vibrational States* (London: Wiley).

CHEN, Y., HALLE, S., JONAS, D. M., KINSEY, J. L., and FIELD, R. W., 1990, *J. opt. Soc. Am.* B, **7**, 1805, and references cited there.

CHILD, M. S., and HALONEN, L., 1984, *Adv. chem. Phys.*, **57**, 1.
CHRISTOFFEL, K., and BRUMER, P., 1986, *Phys. Rev.* A, **33**, 1309.
COLIN DE VERDIERE, Y., 1985, *Commun. math. Phys.*, **102**, 497.
COY, S. L., CHASMAN, D., and FIELD, R. W., 1994, *Molecular dynamics and spectroscopy by stimulated emission pumping*, edited by H.-L. Dai and R. W. Field.
DAVIS, M. J., 1985, *J. chem. Phys.*, **83**, 1016; 1988, *J. phys. Chem.*, **92**, 3124; 1992, *Chem. Phys. Lett.*, **192**, 479; 1993, *J. chem. Phys.*, **98**, 2614; 1994a, *Molecular dynamics and spectroscopy by stimulated emission pumping*, edited by H.-L. Dai and R. W. Field (to be published); 1994b, 'Hierarchical analysis of molecular spectra: Further considerations and a study of energy transfer', (in preparation); 1994c (in preparation).
DAVIS, M. J., and HELLER, E. J., 1981, *J. chem. Phys.*, **75**, 246.
DAVIS, M. J., KOIZUMI, H., SCHATZ, G. C., BRADFORTH, S. E., and NEUMARK, D. M., 1994, *J. chem. Phys.* (submitted).
DAVIS, M. J., MARTENS, C. C., LITTLEJOHN, R. G., and PEHLING, J. S., 1991, *Advances in Molecular Vibrations and Collision Dynamics*, **1***B*, edited by J. M. Bowman and M. A. Ratner (Greenwich: JAI).
DAVIS, M. J., and SKODJE, R. T., 1992, *Advances in Classical Trajectory Methods*, **1**, edited by W. L. Hase (Greenwich: JAI).
DAVIS, M. J., WYATT, R. E., and LEFORESTIER, C., 1982, *Intramolecular Dynamics*, edited by J. Jortner and B. Pullman (Dordrecht: Reidel).
DELON, A., JOST, R., and LOMBARDI, M., 1991, *J. chem. Phys.*, **95**, 5701.
EZRA, G. S., MARTENS, C. C., and FRIED, L. E., 1987, *J. phys. Chem.*, **91**, 3721.
FEINGOLD, M., LITTLEJOHN, R. G., SOLINA, S. B., PEHLING, J. S., and PIRO, O., 1990, *Phys. Lett.* A, **146**, 199.
FISHMAN, S., GREMPEL, D. R., and PRANGE, R. E., 1986, *Phys. Rev.* A, **36**, 289.
FORST, W., 1973, *Theory of Unimolecular Reactions* (New York: Academic).
FREDERICK, J. H., HELLER, E. J., OZMENT, J. L., and PRATT, D. W., 1988, *J. chem. Phys.*, **88**, 2169.
FREED, K. F., 1976, *Top. appl. Phys.*, **15**, 23.
GASPARD, P., and RICE, S. A., 1989a, *J. chem. Phys.*, **90**, 2225; 1989b, *ibid.*, 2242; 1989c, *ibid.*, 2255.
GAZDY, B., and BOWMAN, J. M., 1989, *J. chem. Phys.*, **91**, 4615; 1992, unpublished data.
GIANNONI, M.-J., VOROS, A., and ZINN-JUSTIN, J., editors, 1991, *Chaos and Quantum Physics*, (Amsterdam: North-Holland).
GIBSON, L. L., 1987, PhD thesis, Northwestern University.
GIBSON, L. L., SCHATZ, G. C., RATNER, M. A., and DAVIS, M. J., 1987, *J. chem. Phys.*, **86**, 3263.
GOMEZ LLORENTE, J. M., BORONDO, F., BERENGUER, N., and BENITO, R. M., 1992, *Chem. Phys. Lett.*, **192**, 430.
GOMEZ LLORENTE, J. M., FARANTOS, S. C., HAHN, O., and TAYLOR, H. S., 1990, *J. opt. Soc. Am.* B, **7**, 1851, and references cited there.
GORDY, W., and COOK, R. L., 1984, *Microwave Molecular Spectroscopy* (New York: Wiley).
GRAYCE, B. B., SKODJE, R. T., and HUTSON, J. M., 1993, *J. chem. Phys.*, **98**, 3929.
GUCKENHEIMER, J., and HOLMES, P. J., 1983, *Nonlinear Oscillations, Dynamical Systems, and Bifurcations of Vector Fields* (New York: Springer).
GUTZWILLER, M. C., 1988, *J. phys. Chem.*, **92**, 3154; 1990, *Chaos in Classical and Quantum Mechanics* (New York: Springer).
HAAKE, F., 1991, *Quantum Signatures of Chaos* (Berlin: Springer).
HALLER, E., KOPPEL, H., and CEDERBAUM, L. S., 1983, *Chem. Phys. Lett.*, **101**, 215.
HAMILTON, I., 1990, *J. chem. Phys.*, **93**, 8081.
HASE, W. L., 1976, *Modern Theoretical Chemistry*, edited by W. H. Miller (New York: Plenum).
HENON, M., and WISDOM, J., 1983, *Physica* D, **8**, 157.
HELLER, E. J., 1976, *J. chem. Phys.*, **65**, 1289; 1980, *Ibid.*, **72**, 1337.
HELLER, E. J., STECHEL, E. B., and DAVIS, M. J., 1980, *J. chem. Phys.*, **73**, 4720.
HELLER, E. J., 1984, *Phys. Rev. Lett.*, **53**, 1515; 1991, Giannoni *et al.* (1991).
HOLLAS, J. M., 1982, *High Resolution Spectroscopy* (London: Butterworths).
HUSIMI, K., 1940, *Proc. phys. math. Soc. Japan*, **22**, 264.

JONAS, D. M., SOLINA, S. A. B., RAJARAM, B., SILBEY, R. J., FIELD, R. W., YAMANOUCHI, K., and TSUCHIYA, S., 1992, *J. chem. Phys.*, **97**, 2813; 1993, *Ibid.*, **99**, 7350.

JORTNER, J., RICE, S. A., and HOCHSTRASSER, R. M., 1969, *Adv. Photochem.*, edited by J. N. Pitts, G. S. Hammond and W. A. Noyes, Jr. (New York: Interscience).

KARRLEIN, W., 1991, *J. chem. Phys.*, **94**, 3293.

KELLER, J. B., and RUBINOW, S. I., 1960, *Ann. Phys.*, **9**, 25.

KELLMAN, M. E., 1994, *Molecular Dynamics and Spectroscopy by Stimulated Emission Pumping*, edited by H.-L. Dai and R. W. Field (to be published).

KOIZUMI, H., and SCHATZ, G. C., 1989, *Int. J. quant. Chem.*, **S23**, 137; 1990, *Advances in Molecular Vibration and Collision Dynamics*, I*A*, edited by J. M. Bowman and M. A. Ratner (Greenwich: JAI).

KOIZUMI, H., SCHATZ, G. C., and GORDON, M. S., 1991, *J. chem. Phys.*, **95**, 6421.

LANDAU, L. D., and LIFSHITZ, E. M., 1977, *Quantum Mechanics*, (Oxford: Pergammon).

LEHMANN, K. K., and COY, S. L., 1987, *J. chem. Phys.*, **87**, 5415; 1988, *Ber. Bunsenges. phys. Chem.*, **92**, 306.

LEVINE, R. D., 1988, *Adv. chem. Phys.*, **70**, 53.

LICHTENBERG, A. J., and LIEBERMAN, M. A., 1992, *Regular and Chaotic Dynamics* (New York: Springer).

MCDONALD, S. W., 1983, PhD thesis, University of California.

MCDONALD, S. W., and KAUFMAN, A. N., 1979, *Phys. Rev. Lett.*, **42**, 1189; 1988 *Phys. Rev.* A, **37**, 3067.

MACKAY, R. S., MEISS, J. D., and PERCIVAL, I. C., 1984, *Physica D*, **13**, 55; 1987, *ibid.*, **28**, 1.

MARCUS, R. A., HASE, W. L., and SWAMY, K. N., 1984, *J. phys. Chem.*, **88**, 6717 and references cited.

MARTENS, C. C., and EZRA, G. S., 1987, *J. chem. Phys.*, **87**, 284.

MEISS, J. D., 1992, *Quantum Chaos – Quantum Measurement*, edited by P. Cvitanovic, I. Percival and A. Wirzba (Dordrecht: Kluwer).

METZ, R. B., BRADFORTH, S. E., and NEUMARK, D. M., 1992, *Adv. chem. Phys.*, **81**, 1.

NOID, D. W., KOSZYKOWSKI, M. L., and MARCUS, R. A., 1979, *J. chem. Phys.*, **71**, 2864; 1980, *Chem. Phys. Lett.*, **73**, 269; 1981, *Ann. Rev. phys. Chem.*, **32**, 267.

NOID, D. W., and MARCUS, R. A., 1986, *J. chem. Phys.*, **85**, 3305.

OZORIO DE ALMEIDA, A. M., 1988, *Hamiltonian Systems, Chaos, and Quantization* (New York: Cambridge University Press).

PAPOUSEK, D., and ALIEV, M. R., 1982, *Molecular Vibrational-Rotational Spectra* (New York: Elsevier).

PATE, B. H., LEHMANN, K. K., and SCOLES, G., 1991, *J. chem. Phys.*, **95**, 3891.

PERRY, D. S., 1993, *J. chem. Phys.*, **98**, 6665.

PERSCH, G., MEHDIZADEH, A., DEMTRODER, A., ZIMMERMAN, TH., KOPPEL, H., and CEDERBAUM, L. S., 1988, *Ber. Bunsenges. Phys. Chem.*, **92**, 312.

PIQUE, J. P., 1990, *J. Opt. Soc. Am.* B, **7**, 1816, and references cited there.

RADONS, G., GEISEL, T., and RUBNER, J., 1986, *Phys. Rev. Lett.*, **57**, 2883; 1989, *Adv. chem. Phys.*, **73**, 891.

RADONS, G., and PRANGE, R. E., 1988, *Phys. Rev. Lett.*, **61**, 1691.

REICHL, L. E., 1992, *The Transition to Chaos in Conservative Classical Systems: Quantum Manifestations* (New York: Springer).

ROBINSON, P. J., and HOLBROOK, K. A., 1972, *Unimolecular Reactions* (New York: Wiley).

SADEGHI, R., and SKODJE, R. T., 1993, *J. chem. Phys.*, **99**, 5126.

SCHATZ, G. C., 1990, *J. phys. Chem.*, **94**, 6157.

SCHNIRLMAN, A. I., 1974, *Usp. Mat. Nauk.*, **29**, 181.

SHAPIRO, M., and GOELMAN, G., 1984, *Phys. Rev. Lett.*, **53**, 1714.

SHAPIRO, M., TAYLOR, R. D., and BRUMER, P., 1984, *Chem. Phys. Lett.*, **106**, 325.

SIBERT, E. L., 1990, *Int. Rev. phys. Chem.*, **9**, 1.

SIBERT, E. L., and MAYRHOFER, R. C., 1993, *J. chem. Phys.*, **99**, 937.

STECHEL, E. B., and HELLER, E. J., 1984, *Ann. Rev. phys. Chem.*, **35**, 563 and references cited there.

TABOR, M., 1989, *Chaos and Integrability in Nonlinear Dynamics: An Introduction* (New York: Wiley).

TANG, S. L., ABRAMSON, E. H., and IMRE, D. G., 1991, *J. phys. Chem.*, **95**, 4969.

TAYLOR, R. D., and BRUMER, P., 1983, *Faraday Discuss. chem. Soc.*, **75**, 110.
UZER, T., 1991, *Phys. Rep.*, 199, 73.
WEISSMAN, Y., and JORTNER, J., 1982, *J. chem. Phys.*, **77**, 1486.
YAMANOUCHI, K., IKEDA, N., TSUCHIYA, S., JONAS, D. M., LUNDBERG, J. K., ADAMSON, G. W., and FIELD, R. W., 1991, *J. chem. Phys.*, **95**, 6330.
YAMANOUCHI, K., TAKEUCHI, S., and TSUCHIYA, S., 1990, *J. chem. Phys.*, **92**, 4044.
ZELDITCH, S., 1987, *Duke Math. J.*, **55**, 919.
ZHANG, J., and IMRE, D. G., 1989, *J. chem. Phys.*, **90**, 1666.